Geol. Mag. **150** (*5*), *2013, pp. 862–884.* © *Cambridge University Press 2013*
doi:10.1017/S0016756812000933

Geology, petrology and tectonomagmatic evolution of the plutonic crustal rocks of the Sabzevar ophiolite, NE Iran

MORTEZA KHALATBARI JAFARI*†, HASSAN A. BABAIE‡ & MOJTABA MIRZAIE*

*Research Institute for Earth Sciences, Geological Survey and Mining Exploration of Iran, Tehran, Iran
‡Department of Geosciences, Georgia State University, Atlanta, GA 30302, USA

(*Received* 23 November 2011; *accepted* 17 October 2012; *first published online* 21 March 2013)

Abstract – The plutonic crustal sequence exposed northeast of Sabzevar is part of the ophiolitic belt of Sabzevar that occurs along the northern margin of the Central Iran micro-continent. The sequence includes olivine and pyroxene gabbro with cumulate characteristics, isotropic gabbro, foliated gabbro and a diabase sheeted dyke complex cut by wehrlite and olivine websterite intrusions, and pegmatite gabbro and plagiogranite as small intrusions and dykes. The sequence is comparable to gabbros in known ophiolite complexes. Microscopic studies show an abundance of the mesocumulate and heteradcumulate textures that represent open system magma chambers, which are common in supra-subduction zones. The olivine → plagioclase → clinopyroxene → ± orthopyroxene → amphibole trend of mineralization in the gabbros, similar to mid-ocean ridge basalt (MORB), and olivine → clinopyroxene → ± orthopyroxene → plagioclase → amphibole, similar to arc rocks, indicate the diversity in the formation of these rocks, and represent petrographic evidence of their formation in a supra-subduction zone. The rocks have calc-alkaline to tholeiitic affinities, and niobium depletion in the spider diagrams of diabase that matches the patterns of island arc magma. These patterns, and the light rare earth element enrichment of the diabase and plagiogranite, suggest the effect and introduction of the fluids, originating from the subducting slab, beneath the mantle wedge. The low titanium compositions, matching those of arc diabase and plagiogranite, plot in the island arc to MORB tectonomagmatic fields, and suggest formation of the Sabzevar ophiolitic plutonic crustal sequence in a supra-subduction zone during Late Cretaceous time.

Keywords: gabbro, cumulate, mesocumulate, heteradcumulate, MORB, supra-subduction.

1. Introduction

The studied ophiolitic plutonic crustal sequence, exposed north and northeast of Sabzevar, between 57° 44′ E and 58° 00′ E longitude, and 36° 22′ N and 36° 16′ N latitude, is part of the Sabzevar ophiolite belt that occurs around the Central Iran micro-continent (Fig. 1) (Stocklin, 1968; Knipper & Ricou, 1986). The ophiolite, with a general E–W trend, starts from around the town of Fariman in the east, and extends, as tectonic slices, to near Abbasabad village where it narrows and disappears. The Sabzevar ophiolite is exposed along the Meyamey Fault between the Central Iran micro-continent and the Alborz–Binalud structural zone (Fig. 1).

Earlier study of the ophiolite belt, in the form of Ph.D. dissertation (E. Sadredini, unpub. Ph.D. thesis, Univ. Saarbrucken, 1974), described the geology and petrography of the middle part of the Sabzevar ophiolitic belt, with a 1:200 000 geological map, in an area between the villages of Bid in the west and Ooz in the east. Although the map presented various units of ophiolitic sequences, such as a diabase sheeted dyke complex in Bagjar and a gabbroic body in Soleymanieh, it did not cover the wehrlitic intrusion, pegmatite gabbro and plagiogranite. F. Vaziri-Tabar (unpub. Ph.D. thesis, Univ. Saarbrucken, 1976) determined the microfauna in the pelagic limestone and described the petrography of phyric andesite in the Upper Cretaceous turbiditic series and Eocene volcanic sedimentary rocks northwest of Sabzevar. N. Alavi-Tehrani (unpub. Ph.D. thesis, Univ. Saarbrucken, 1976) studied the geology and petrography of the ophiolitic rocks northwest of Sabzevar with a 1:250 000 geological map covering an area between the villages of Tabas in the east and Bid in the west. He described the geochemistry of different rocks from the Sabzevar ophiolitic sequences and concluded that they are not the product of a single magmatic activity, and proposed an oceanic ridge model for their formation. Lensch, Mihm & Alavi-Tehrani (1977) interpreted the geology and petrography of the Sabzevar ophiolite in a geological map at the scale of 1:500 000. They distinguished eight main units in the ophiolitic belt: harzburgite, intrusive rocks, a sheeted dyke complex, volcanic sedimentary sequences, mélange, metamorphic rocks, a Tertiary series and Quaternary rocks. However, their work did not describe the wehrlitic intrusion. Lensch, Mihm & Alavi-Tehrani (1979, 1980) and Lensch (1980), studying 230 major element chemical analyses, recognized the low-Ti character of the ophiolitic crustal rocks and attributed them to an immature island arc. Lensch & Davoudzadeh (1981) identified three types of ophiolitic assemblage around the Central Iran micro-continent: a ridge type, trench type and coloured mélange. According to their palaeontological data, the

†Author for correspondence: khalat1965@live.com

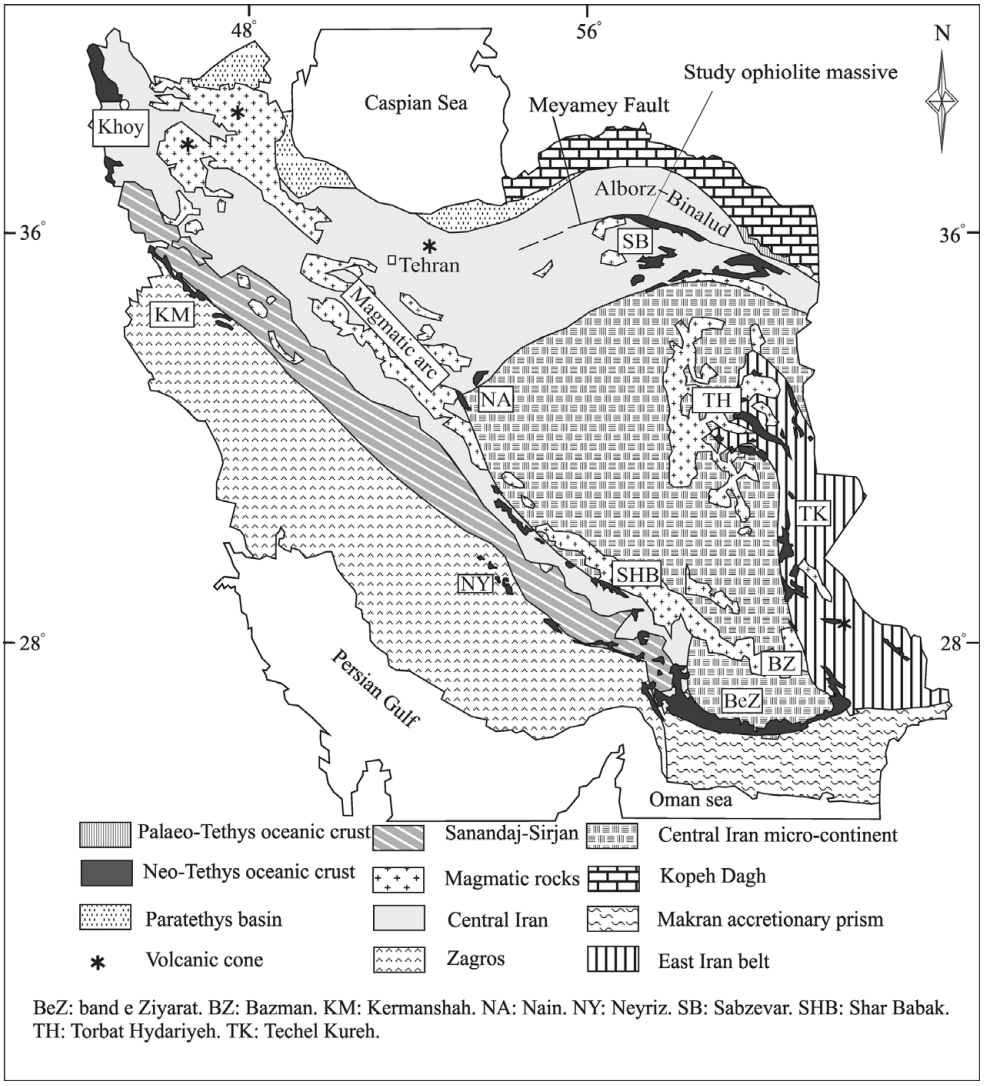

Figure 1. Map showing the distribution of the exposures of ophiolites in Iran and the location of the study area. Adapted from 1:1 000 000 Magmatic Map of Iran by Emami, Sadegi & Omrani (1993) and Sedimentary–Structural Map of Iran by A. Aghanabati (2004).

ophiolitic sediments are Campanian–Maastrichtian in age. Radiometric (K–Ar) age determination yielded 81.2 ± 4.1 Ma and 76.8 ± 3.8 Ma ages for the lava and diabase (Lensch & Davoudzadeh, 1981). The trench type ophiolite is exposed in two large massifs south of Sabzevar, at Oryan and north of Bardeskan. The ridge type is exposed in the northern part of the belt (Lensch, Mihm & Alavi-Tehrani, 1979, 1980). The highly deformed coloured mélange is exposed near the city of Nain. In another dissertation project, M. K. Noghreyan (unpub. These ès Sciences, Univ. de Nancy I, France, 1982) studied the geochemical, mineralogical and structural evolution of the middle part of the ophiolite complex. He described the deformation in harzburgite and proposed that differentiation in the cumulate gabbro occurred in a closed magma chamber. He further proposed that fractional crystallization occurred from a tholeiitic magma that was enriched in silica and had low values of titanium. Applying the discrimination geochemical diagrams from hypabyssal volcanic rocks, Noghreyan (unpub. These ès Sciences, Univ. de Nancy I, France, 1982) suggested that the ophiolitic belt formed in relation to an immature arc. Ohnenstetter (1983) studied the layered cumulate gabbro in Soleymanieh (Fig. 2) and Tabas and Nurabad massifs, and interpreted them to be a disrupted magma chamber. Based on her structural study of the layered cumulate gabbro, she concluded that accretion occurred along an oblique spreading axis. Her structural investigation revealed that the shape of the magma chamber and layering in the gabbro massifs were mainly controlled by faults. Lindenberg, Goerker & Ibbeken (1983) reported structural and orogenic evolution of the Sabzevar ophiolite belt in the area of Oryan. In their model, the ophiolitic mélange in Oryan is interpreted as tectonized breccia at the base of the oldest nappes. Spices, Lensch & Miham (1983) studied the geochemistry of the post-ophiolitic Tertiary volcanic rocks between Sabzevar and Quchan/NE Iran, and suggested a geodynamic model for a collision between an oceanic lithosphere and oceanic island arc, with andesitic volcanism along the continental margin

https://doi.org/10.1017/S0016756812000933 Published online by Cambridge University Press

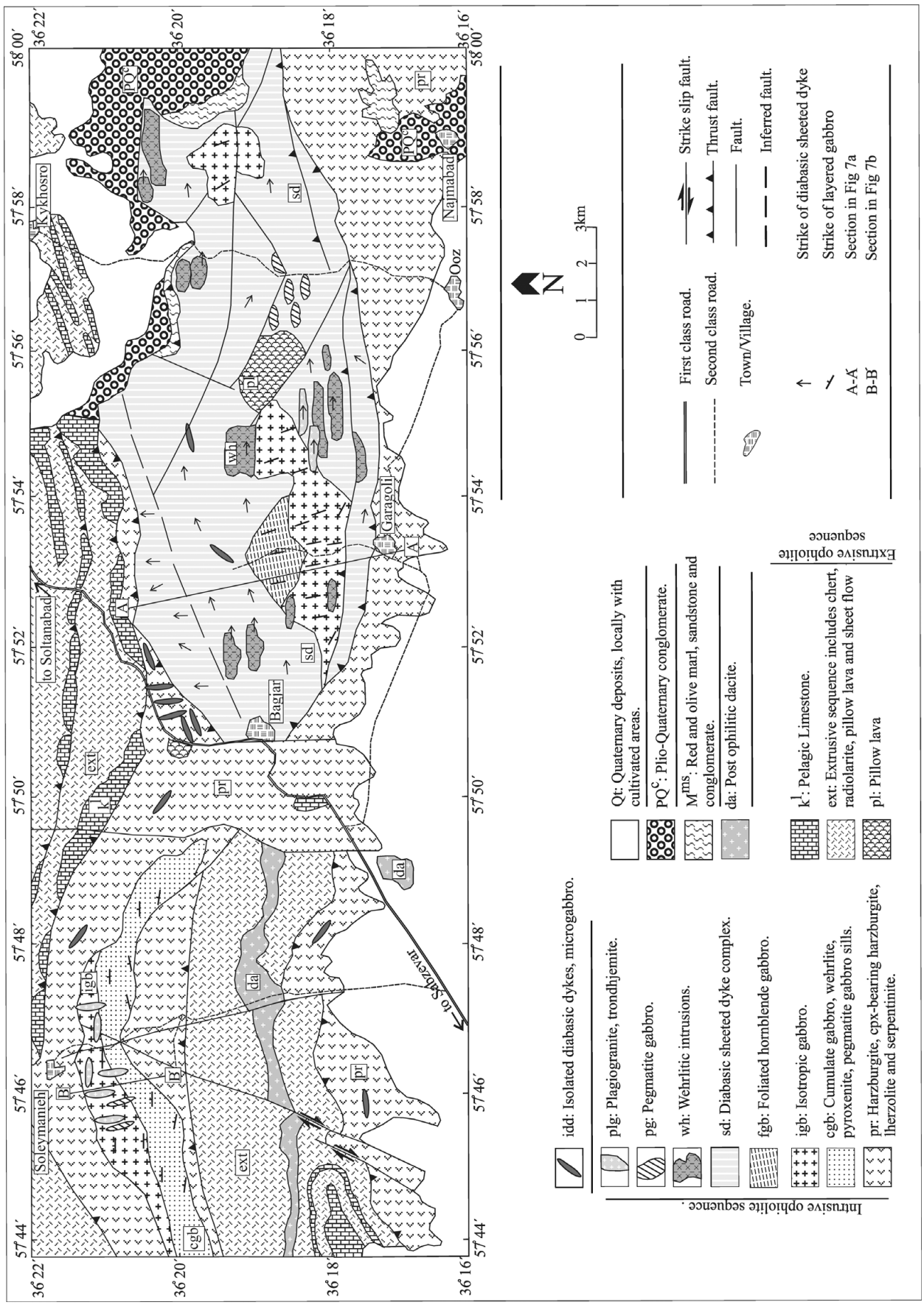

Figure 2. Reduced (1:75 000) version of our 1:25 000 geological map of the study area.

https://doi.org/10.1017/S0016756812000933 Published online by Cambridge University Press

of the Turan plate. In their hypothesis, the closure of the rift took place in the Eocene between the central-East Iran microplate and Turan plate. Post-ophiolitic calc-alkaline volcanism was generated by partial melting of the mantle wedge above a northwardly directed subduction zone. Baroz *et al*. (1984) discussed the possible geotectonic reconstructions of the middle part of the Sabzevar ophiolite and, by attributing the composition of pillow lavas to immature island arcs (Lensch, Mihm & Alavi-Tehrani, 1979, 1980), suggested formation at an active margin. The 1:250 000 Sabzevar Geological Quadrangle (compiled by Sahandi, 1992) and 1:100 000 Sabzevar Geological Quadrangle (Majidi, 1999) are published by the Geological Survey and Mineral Exploration of Iran (Fig. 2). Shojaat *et al*. (2002) investigated the petrology, geochemistry and tectonics of the Sabzevar ophiolite. They distinguished basaltic rocks that formed from an initial melt with a normal mid-ocean ridge basalt (N-MORB) chemical signature, enriched MORB (E-MORB) and basaltic rocks with a light rare earth element (LREE)-enriched signature, and incompatible trace element patterns that suggest an island arc affinity. Rossetti *et al*. (2009) assigned an Early Cretaceous (Albian) isotopic age for the peak of metamorphism around Soltan Abad.

Although the geological map of Lensch, Mihm & Alavi-Tehrani (1977) shows the diabase sheeted dyke complex of the north Garagoli–Ooz area, it misses the wehrlitic and pegmatite gabbro intrusions. The sheeted dyke complex is introduced as a micrograbbro on the geological map of Majidi (1999). A comparison of the change in the strike of the sheeted diabase dykes and layering in the Soleymanieh (Ohnenstetter, 1983) and Garagoli gabbroic plutons necessitates the revision of the geology in the study area. The absence of minor and REE data from these rocks, and their interpretation based on the new definition of ophiolites, given approximately after the introduction of supra-subduction ophiolites (Pearce, Lippard & Roberts, 1984), also calls for a study of the ophiolitic plutonic crustal sequence in the area northeast of Sabzevar. To study the plutonic crustal sequence, we selected a section in the valley north of Garagoli (Fig. 2) and, for comparison, systematically sampled the gabbro exposed to the south of Soleymanieh village. Samples of wehrlite and plagiogranite northwest of Ooz and south of Kykhosro villages (Fig. 2) were also collected. After preparing the thin-sections and subsequent petrographic study, 20 unaltered samples were selected and sent to the SGS Laboratory in Canada (http://www.sgs.com/en/Mining) for analysis of major oxides and minor and trace elements with the inductively coupled plasma mass spectrometry (ICP-MS) and inductively coupled plasma atomic emission spectroscopy (ICP-AES) methods.

2. Geology

Figure 2 shows the reduced (1:75 000) version of our new 1:25 000 geological map of the area. Although the contact between the intrusive and extrusive sequences is tectonic, the transition from the isotropic gabbro to the diabase sheeted dykes is normal. The mantle sequence in the study area comprises harzburgite, clinopyroxene-bearing harzburgite, lherzolite, serpentinized dunite and local lenses of chromitite. Despite pervasive serpentinization of the peridotite, in some cases the porphyroclastic texture is still apparent where large crystals of orthopyroxene and rotated clinopyroxene occur in a groundmass of serpentinized olivine, producing a foliation. Petrographic study reveals the presence of kink bands in large olivine crystals. The strike of the foliation is variable and hard to follow owing to intense deformation and serpentinization, but the approximate dip is subvertical to the north. In some cases, the peridotite is cut by individual, often rodingitized diabasic to gabbroic and micrograbbroic dykes along N–S, E–W and occasionally NW–SE directions. Serpentinite, with remnants of chert, radiolarite, fragmented pillow lava and sparse listvenite occur along thrust zones in an area northwest of Ooz and east of Garagoli villages (Fig. 2). These chaotic serpentinites do not show any sign of metamorphism, foliation or lineation. Therefore, they can hardly be categorized as 'coloured melange' as defined by the Penrose Committee (Anonymous, 1972). Subvertical–vertical, few centimetre thick veins and veinlets of pyroxenite cut across the peridotite. Ohnenstetter (1983) reported 50 cm thick pyroxenite dykes that cut serpentinized peridotite and have dunite margins. Chromitite lenses also occur, west of Ooz and north of Bagjer village, with remnants of intensely serpentinized dunite. The relationship between dunite and chromitite cannot be deciphered because of mining excavations. Occasionally, the peridotite is intensely tectonized, and contains exotic blocks of mylonitic granite and amphibolite.

Exotic blocks of amphibolite and mylonitic granite, exposed north of Bagjer, may be tectonic remnants of the Soltan Abad metamorphic complex (Rosetti *et al*. 2009), which is exposed north of the Sabzevar ophiolite belt. These blocks have been metamorphosed up to greenschist facies, and are composed of intermittent, dark slivers of metabasite-amphibolite and light granitic mylonite. The layers are a few millimetres to a few centimetres in thickness, and are folded in places. Amphiboles, mostly actinolite, define a foliation in the dark layers. Mylonitic texture and structure are apparent in the light layers, with altered quartz and plagioclase porphyroclasts.

South of Soleymanieh, the plutonic crustal sequence contains layers of olivine gabbro, with cumulative characteristics, and pyroxene gabbro, wehrlite-pyroxenite and pegmatite gabbro in the base, and massive and isotropic gabbro at the top of the body, which are intruded by pegmatite gabbro and plagiogranite veins and isolated diabasic dykes. In Garagoli, cumulate gabbro is scarce, but massive and isotropic gabbro with faint layering occurs at the base. Foliated hornblende gabbro occurs at the top and grades to the diabase sheeted dyke complex. Both are cut, at low angles to

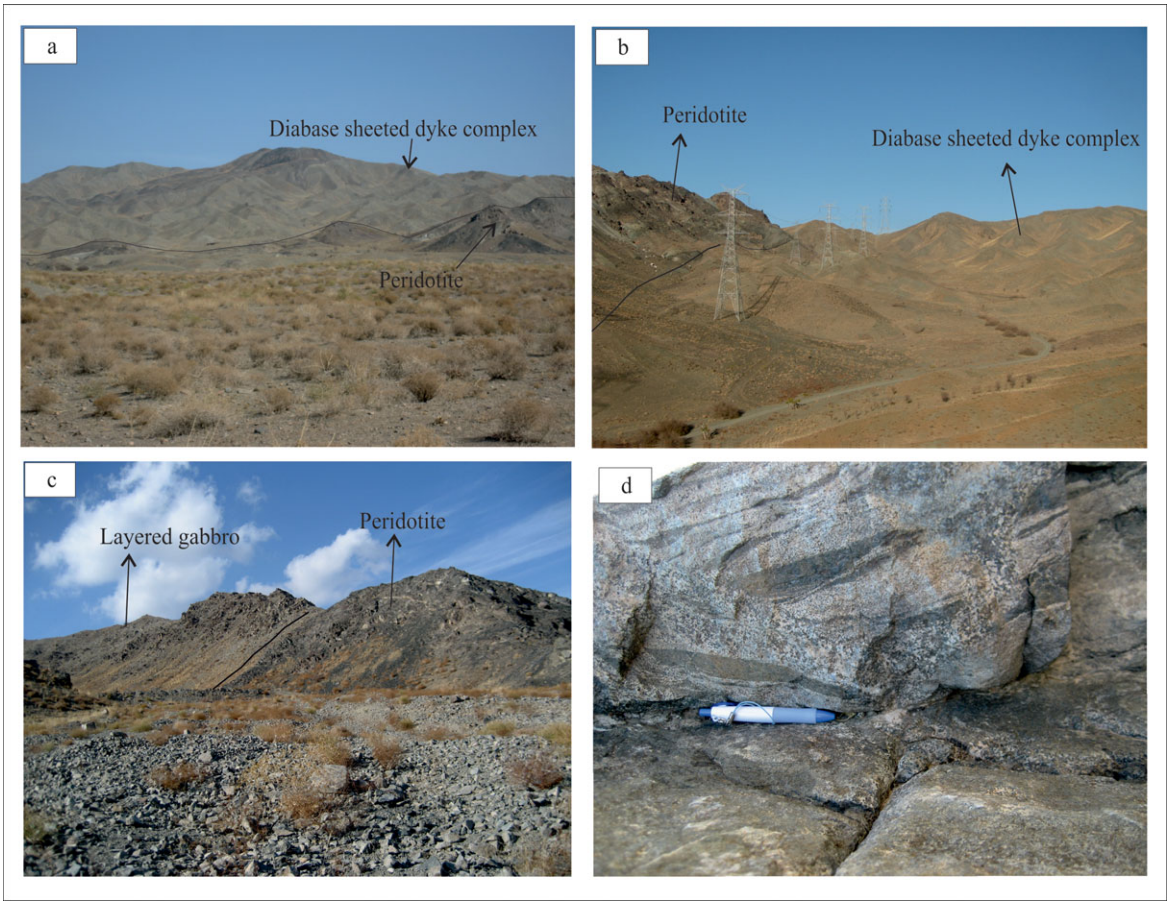

Figure 3. (Colour online) Selected field pictures. (a) A perspective from a distance, showing the thrusting of the diabase sheeted dyke complex over peridotite, northwest of Garagoli village. (b) Thrusting of peridotite onto the diabase sheeted dyke complex, northeast of Bagjer village. (c) Peridotite underlying layered and cumulate gabbro with a tectonized contact, exposed southwest of Soleymanieh village. (d) Magmatic layering in the cumulate gabbro, southwest of Soleymanieh. Pen is 14 cm long.

the layering, by individual diabase dykes, wehrlite and olivine websterite intrusions, and pegmatitic gabbro and plagiogranite veinlets and pseudosills. Figures 3–6 show selected field features and Figure 7 depicts the geological sections of the plutonic crustal sequence north of Garagoli (Fig. 7a) and south of Soleymanieh (Fig. 7b) villages. Rose diagrams, displaying the trend of the dominant planar features in each unit, are also shown in Figure 7. Figure 8 shows the schematic stratigraphic column of the plutonic crustal sequence north of Sabzevar.

Different units occur in tectonic slices that are bound on both sides by thrusts. Southwest of Garagoli, the diabase sheeted dykes are thrust onto serpentinized peridotite (Fig. 3a), and in the northeast of Bagjer village, peridotite is thrust onto the sheeted dykes (Fig. 3b). The thrusts dip to the north and the thrust units in the sequence grade into one another from the bottom to the top; for example, the massive gabbro grades into the diabase sheeted dyke complex. In the area east of Garagoli, the cumulate gabbro is scarce and occurs with wehrlite intrusions, but exhibits better outcrops south of Soleymanieh (Fig. 3c). In the Soleymanieh area, the cumulate gabbro and pyroxene gabbro are exposed and have magmatic layering (Fig. 3d) and marked shear zones showing ductile deformation. The gabbro has plenty of light and dark bands of plagioclase and ferromagnesian minerals, respectively, which are cut, at very low angles to the layering, by thin layers of pyroxenite, pseudosills of pegmatitic gabbro and plagiogranite (Fig. 4a, b).

The thickness of the layers in the Soleymanieh gabbro ranges from a few centimetres to 0.75 cm. Wehrlite and pyroxenite occur in thin (few centimetre) discontinuous sills in the cumulate gabbro. Pegmatite gabbro also occurs as sills with olivine gabbro, but its mineralogy differs from the pegmatite gabbro that occurs as fine veins and dykes that cut the isotropic gabbro at the top of the body. While olivine crystals in the layered pegmatite gabbro constitute the primary minerals, those in the pegmatite gabbro veins are scarce or not seen at all. The pyroxenes in the pegmatite gabbro at the base of the Soleymanieh body are clinopyroxene and, in places, orthopyroxene, and are often substituted in the veins by amphiboles. Mineralogic granometric variation is not seen in every layer, and a transition from olivine gabbro to pegmatite gabbro or layers of wehrlite and pyroxenite does not occur, which may be explained by sequential injections of mafic magma into the magma chamber.

The base of the cumulate layers in the Soleymanieh body strike approximately E–W with a few degrees

https://doi.org/10.1017/S0016756812000933 Published online by Cambridge University Press

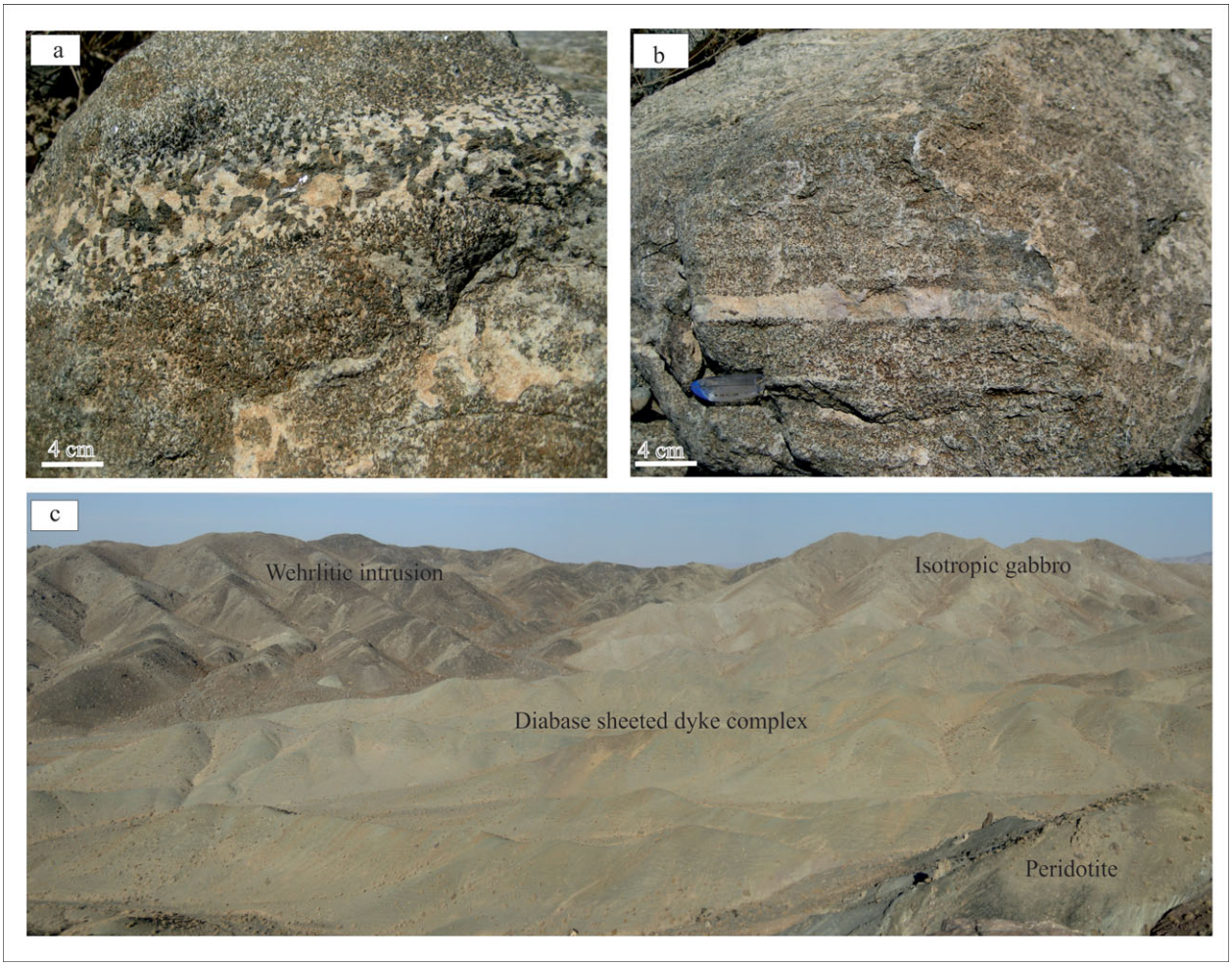

Figure 4. (Colour online) Selected field pictures. (a) Pseudosills of pegmatite gabbro parallel to the magmatic layering. (b) Formation of plagiogranite along the magmatic layering in the layered gabbro, southwest of Soleymanieh. (c) Exposure of the isotropic gabbro, diabase sheeted dykes and wehrlitic sills, south of Kykhosro village.

of variation. The variation is greater at the contact between the body and the peridotite country rock. The layering disappears or becomes sparse at the top of the body and in the isotropic gabbro. Only the trace of the layers can be measured on two-dimensional exposed surfaces, making it difficult or impossible to determine the dip of the layers. For this reason, the dips shown on the sections in Figure 7 are estimated. The majority of the pegmatite gabbro and plagiogranite veins strike N–S, with a few that strike E–W. A small number of individual diabase dykes cut the Soleymanieh gabbro. Although cumulate gabbro is exposed south of Soleymanieh, where it grades into isotropic gabbro at the top of the sequence, its outcrops are scarce in Garagoli and south Kykhosro. In these two areas, massive and foliated hornblende gabbro and a diabase sheeted dyke complex, which correlate with the upper parts of gabbros in well-known ophiolites such as Oman (Nicolas & Boudier, 2009), are predominant (Fig. 4c).

The isotropic gabbro in the Garagoli body shows mineralogical similarities to the isotropic gabbro at the top of the south Soleymanieh gabbroic body. In both, olivine disappears and clinopyroxene and plagioclase gradually increase towards the top of the body. The magmatic layering also gradually disappears towards the top in both bodies. The dominantly N–S-striking layers of the Garagoli body differ from the mostly E–W-striking layers in the Soleymanieh body, and show evidence for plastic and viscous deformation superposed on magmatic layering. The obliteration of magmatic layering increases towards the middle of the body, where it becomes difficult to measure the attitude of the layers. Wedge- and arrow-shaped and twisted light-coloured layers of mostly plagioclase and dark layers of pyroxene and occasional olivine give evidence for plastic deformation.

North of Garagoli, foliated hornblende gabbro occurs above the massive and isotropic gabbro (Fig. 8), and evidence for the root of the diabase sheeted dykes is first observed in the foliated and isotropic gabbro. Plagioclase, clinopyroxene and hornblende display a clear preferred orientation in the foliated gabbro. However, in known ophiolites such as Oman, the succession is layered gabbro, followed by foliated gabbro, with steep foliation that parallels dykes in the sheeted dyke complex, followed by a thin layer of isotropic gabbro and plagiogranite in which the

https://doi.org/10.1017/S0016756812000933 Published online by Cambridge University Press

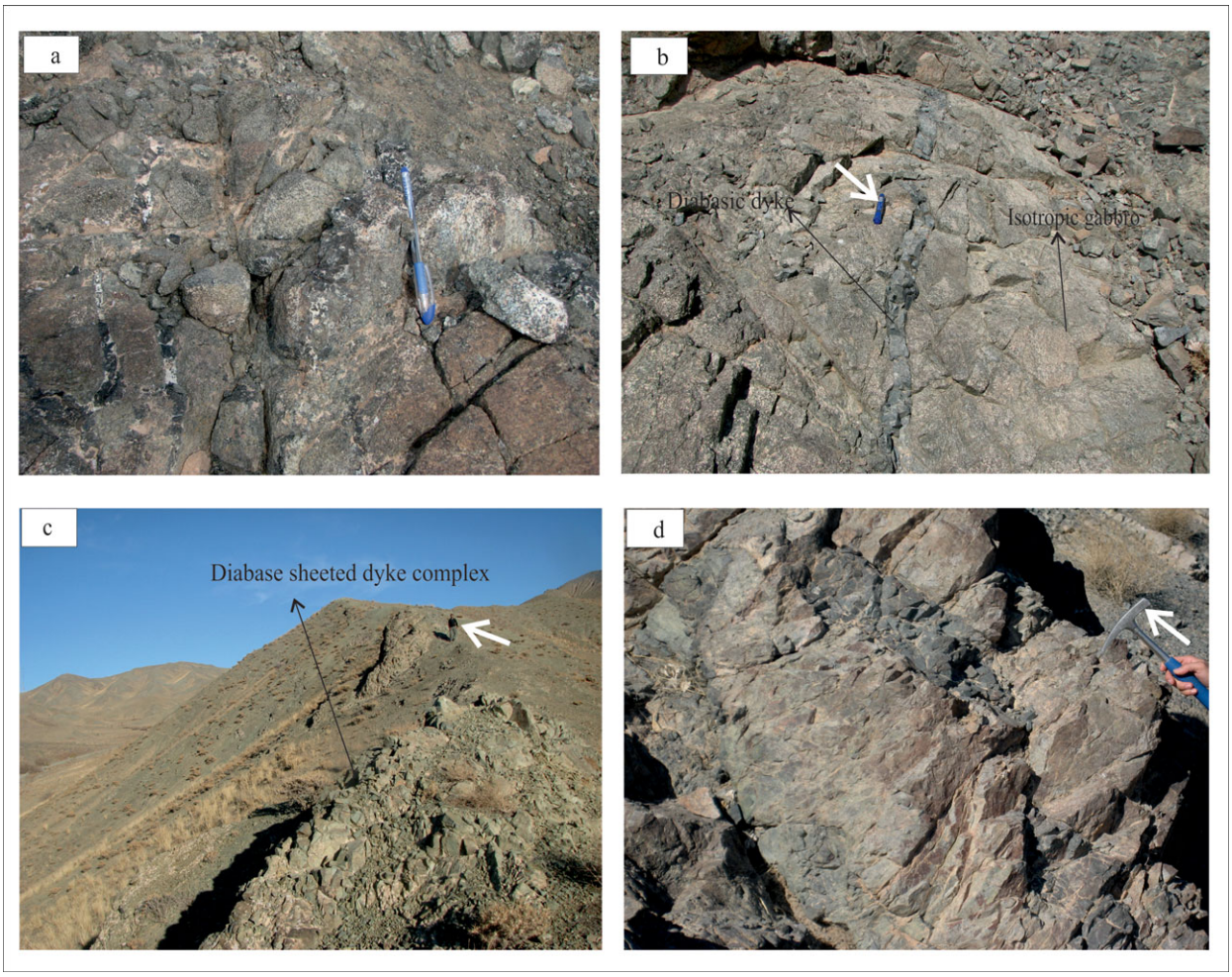

Figure 5. (Colour online) Selected field pictures. (a, b) Pegmatite gabbro veins, plagiogranite and individual diabase dykes (b), cutting the isotropic gabbro north of Garagoli. Pens for scale are 12 cm long. (c) Diabase sheeted dykes north of Garagoli. Height of man for scale is 160 cm. (d) Coarse-grained and microcrystalline (darker layer) diabase, west of Ooz village. Hammer for scale is 32 cm long.

sheeted dyke complex is rooted (Nicolas & Boudier, 2009; Juteau & Mury, 2009). The magmatic foliation in the foliated hornblende gabbro in the Garagoli body, which lies above the isotropic gabbro, is primary and viscous and, in contrast to the middle part of the body, does not show any evidence for plastic deformation. Moreover, the strike of the foliation in the foliated hornblende gabbro is oriented N–S, similar to the faint layering in the isotropic gabbro. Further studies are required to understand the differences between the foliated gabbro in known ophiolite sequences in Oman and foliated hornblende gabbro in the Garagoli body. As has been suggested for ophiolitic hornblende gabbro from the central Anatolian Aksaray and Kayseri regions in Turkey (Kocak *et al*. 2005), such a gabbro may have formed from a hydrous peridotite source. The massive gabbro is cut by veinlets of pegmatite gabbro (Fig. 5a), plagiogranite, and less frequently, individual diabase, microgabbro and andesitic-basaltic dykes (Fig. 5b). The diabase sheeted dykes (Fig. 5c) occur as coarse and fine crystal facies types (Fig. 5d).

The diabase sheeted dykes strike approximately E–W north of Garagoli and N–S in the area northeast of Bagjer village (Fig. 2). Wehrlitic intrusions cut these units (Fig. 6a–c), and form dark and high peaks northwest and east of Garagoli. Small (millimetre-scale) quartzo-feldspathic aggregates occur in the wehrlitic intrusions, north of Ooz. The formation of these aggregates may signify differentiation of plagiogranite from wehrlite, a hypothesis that requires further field and laboratory investigation. The margins of these wehrlitic intrusions are completely lobed (Fig. 6b) and intercalated, suggesting that they were intruded into the country rock occurred while they were warm and viscous. The contacts of the intrusion with the isotropic gabbro and diabase sheeted dykes, on the other hand, show alteration zones. North of Garagoli, the pegmatite gabbro occurs as small bodies, and often as vein-veinlets that cut peridotite, gabbro, diabase sheeted dykes and wehrlitic intrusions. The pegmatite gabbro, in this area, often includes clinopyroxene, plagioclase, amphibole and rarely olivine. In massive types, the often rodingitized clinopyroxene crystals may reach 40 cm in length. The plagiogranite occurs as small bodies (Fig. 6d) or parallel dykes that cut wehrlitic and pegmatitic gabbro intrusions. Like the wehrlitic intrusions, plagiogranites occur along E–W-oriented exposures northwest of Ooz and south of Kykhosro (Fig. 6d).

https://doi.org/10.1017/S0016756812000933 Published online by Cambridge University Press

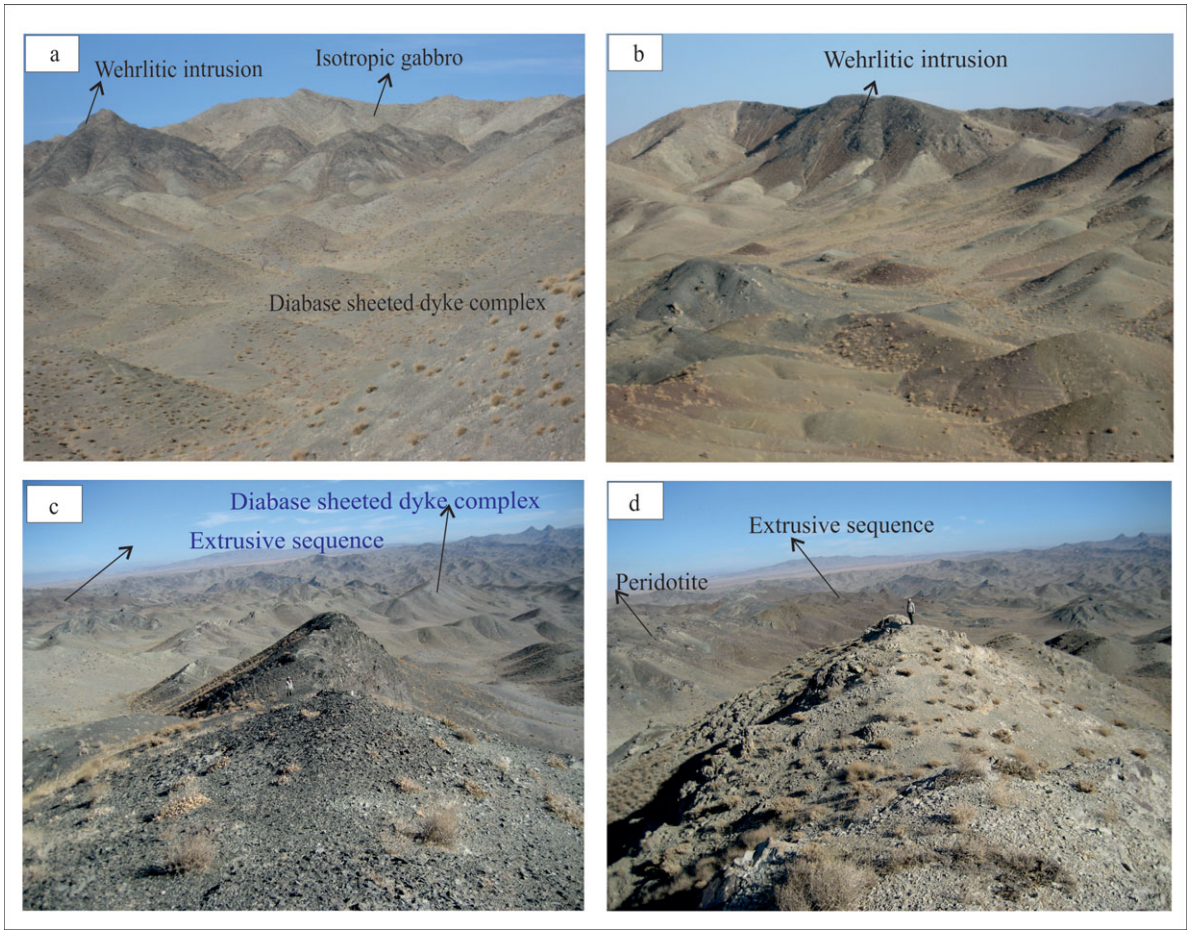

Figure 6. (Colour online) Selected field pictures. (a) E–W-trending exposure of the wehrlite intrusion cutting the isotropic gabbro and diabase sheeted dykes, west of Ooz. (b) A wehrlite intrusion with lobed margins, cutting the diabase sheeted dyke complex, east of Garagoli. (c) E–W-trending wehrlite intrusion east of Garagoli (looking east). (d) E–W-trending plagiogranite exposure (looking east).

Figure 7c schematically illustrates opening across the axis of a mid-ocean ridge and segmentation of the ridge along transform faults (Juteau & Maury, 2009). While the sheeted dykes form parallel to the ridge axis, in these environments, the foliation (banding) in the cumulate gabbro and the mineral preferred orientation in the foliated gabbro, develop perpendicular to the ridge (Juteau & Maury, 2009). These orientations may deform (rotate) by transform faults as much as 90°. Structural analysis of the strike of the magmatic layering and the strike of the diabase dykes in the area north of Garagoli, and their comparison with the strike of the magmatic layering in the area south of Soleymanieh, provide important clues to test this model. North of Garagoli, the magmatic layering in the gabbro and mineral preferred orientations in the foliated hornblende gabbro are oriented roughly N–S. The diabase dykes and outcrops of plagiogranite and wehrlite are oriented approximately E–W (Fig. 7a). The diabase sheeted and individual dykes, in the same area, also strike approximately E–W, across the magmatic layering in the gabbros. These measurements, taken north of Garagoli, suggest an opening across an E–W-oriented mid-ocean ridge. On the other hand, in the area south of Soleymanieh, the magmatic layering roughly strikes E–W, and gabbro veinlets of pegmatite and plagiogranite strike N–S (Fig. 7b). If the pegmatite veinlets form parallel to the ridge axis, a N–S trend for the ridge axis can be inferred in the Soleymanieh area. The discrepancy in the orientation of the inferred ridge axes in the two areas can be explained either by rotation during emplacement of the ophiolite or by transform faults (Fig. 7c). The latter is suggested by deformation indicators such as those in mylonitic harzburgite, characterized by stretched, elongated olivine bands deformed by systematic kink bands, and rotated and bent diopside porphyroclasts with undulose extinction. Determination of the true trend of the ridge in the Sabzevar ophiolite belt requires extensive and systematic measurement of the attitude of magmatic and shear-related foliation and lineation in the area between the wide exposures of the ophiolite at its starting point around the town of Fariman in the east and Abbasabad village in the west where it tapers off.

North of Bagjer village, volcanic rocks, which occasionally form ridges, occur at the top of the extrusive sequence of the Sabzevar ophiolite (Fig. 8), and contain pillow lava with minor volcaniclastic rocks, mainly tuff and breccia, and pelagic limestone. Hyaloclastic breccia with carbonate cement and interlayers of pelagic limestone occur as intercalations among the pillow lava.

https://doi.org/10.1017/S0016756812000933 Published online by Cambridge University Press

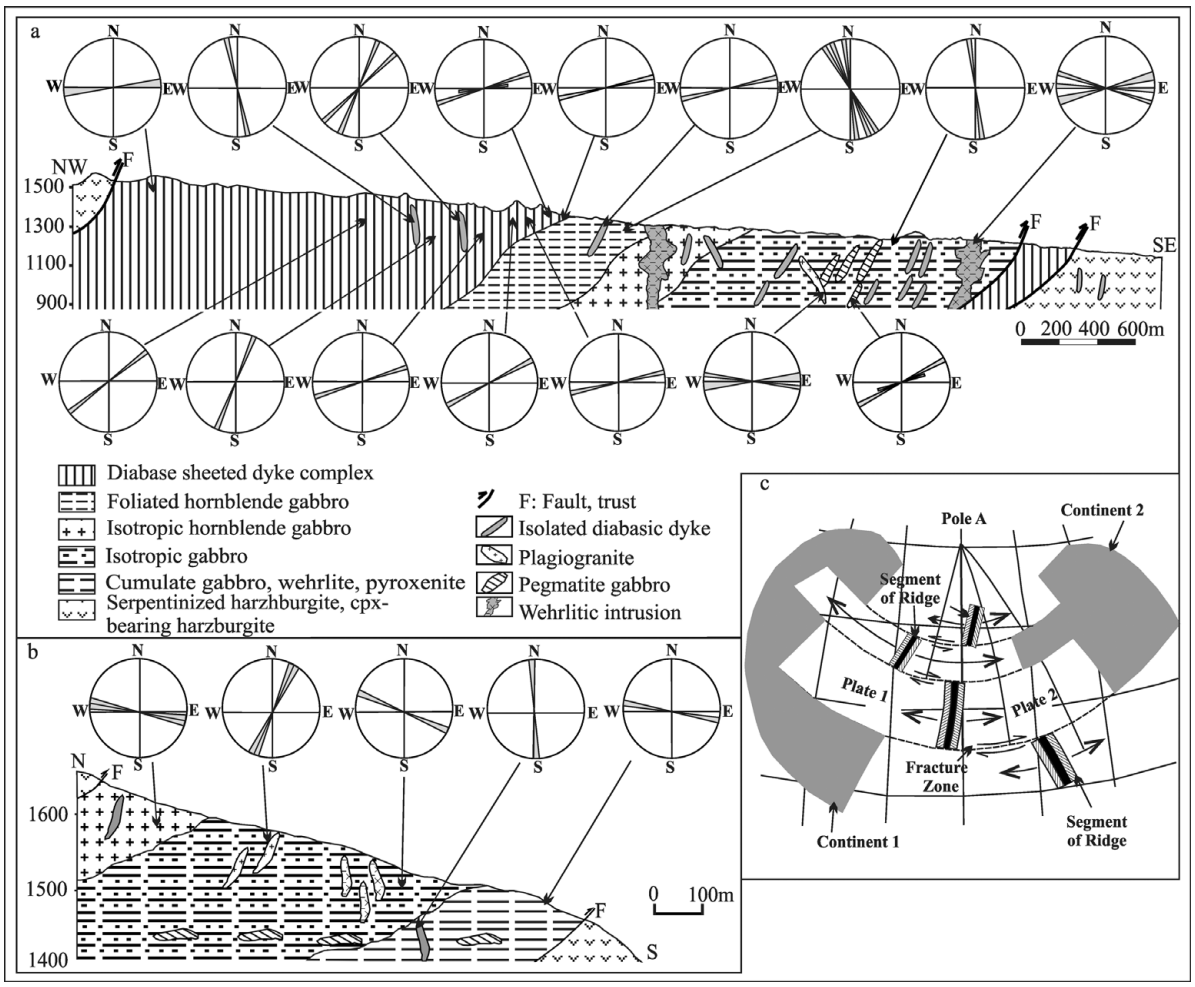

Figure 7. Geological sections across the crustal sequence, with corresponding rose diagrams shown for each unit, (a) north of Garagoli village, and (b) southwest of Soleymanieh. (c) Schematic diagram depicting the opening of the mid-ocean ridge and movement along transform faults.

Palaeontological study of the pelagic limestone by Zohreh Sohrabi (unpub. report, Geological Survey of Iran, 2009) at the Geological Survey and Mining Exploration of Iran, assigned a Late Cretaceous age (Maastrichtian – Late Maastrichtian), which represents the relative age of the ophiolite in this area. The following microfauna is identified in the pelagic limestone: *Abathomphalus mayaroensis, Racemiguembelina fructicosa*, *Gansserina gansseri*, *Trinitella scotti*, *Globotruncanita stuarti*, *Globotruncanita stuartiformis*, *Globotruncana* aff. *falsostuarti*, *Globotruncanita conica*, *Radotruncana calcarata*, *Contusotruncana atelliformis*, *Pseudotextularia nuttalli* and *Heterohelix* sp.

3. Petrography

Petrographic investigation shows that the cumulate gabbros, including olivine and pyroxene gabbro, occur with thin layers of pyroxenite. The olivine gabbro has a microscopic mesocumulate texture, while pyroxene gabbro has an adcumulate texture. Heteradcumulate and granular textures are also seen in the upper parts of the massive gabbro. The layering in the cumulate rocks is defined by the internal variation of the amount of the modal minerals in each layer (Hunter, 1996). The term 'cumulate' was defined by Wager, Brown & Wadsworth (1960), and used by Wager (1963) and Wager & Brown (1968) to describe the texture of layered and cumulate igneous rocks whose minerals had cooled slowly. In this definition, early crystals that crystallize on the floor of the magma chamber are called cumulus and those that form out of the interstitial liquids are called intercumulus.

The olivine gabbro contains olivine, clinopyroxene, orthopyroxene and plagioclase. The olivine is the cumulus phase and occurs as anhedral crystals with a high relief and many fractures along which olivine is altered to serpentine. In places, olivine is completely altered to serpentine, which may constitute about 10–15 % of the rock. Kink bands (Fig. 9a) also occur in the olivine, suggesting compaction during viscous deformation (Hunter, 1966). Olivine inclusions in plagioclase (Fig. 9b), clinopyroxene (Fig. 9c) and orthopyroxene (Fig. 9d) indicate earlier formation of olivine compared to the host minerals. Plagioclase has albite, Carlsbad and arrowhead twinning, and calcic compositions, ranging from labradorite to bytownite, and constitutes 45–50 % of the thin-section. The albite twinning is pointed in places and looks like the

https://doi.org/10.1017/S0016756812000933 Published online by Cambridge University Press

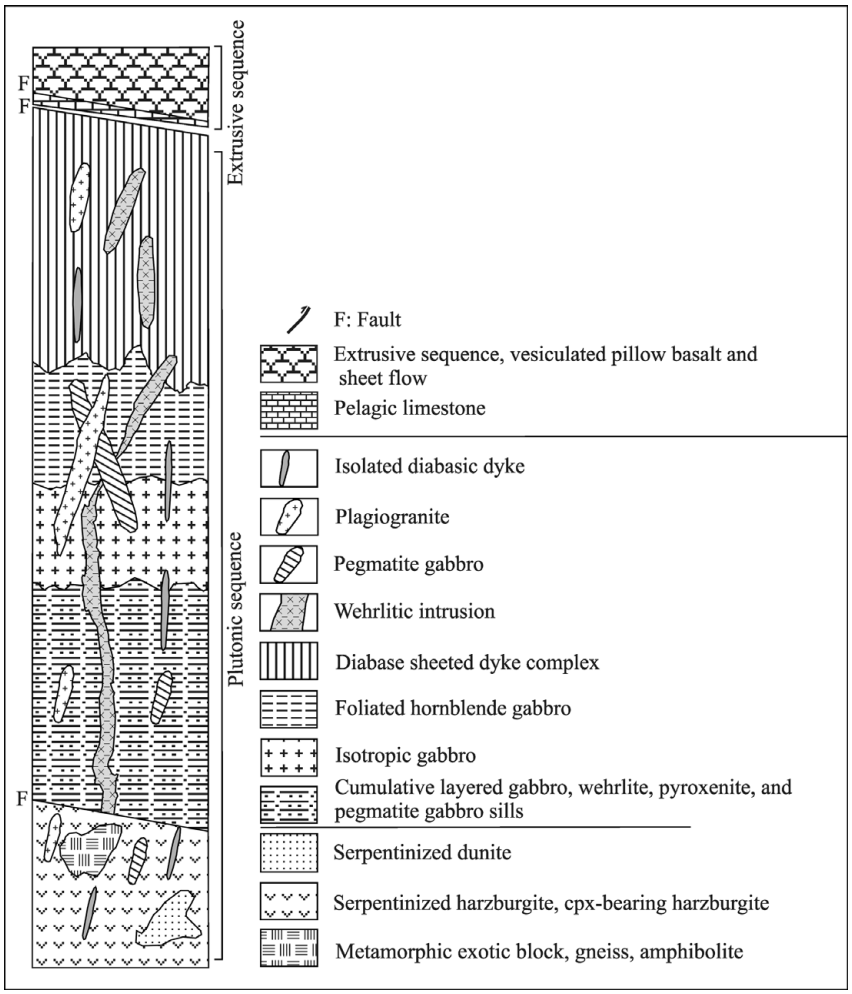

Figure 8. Schematic stratigraphic column of the plutonic crustal sequence, north of Sabzevar.

arrowhead twinning (Fig. 9b). This kind of twinning in plagioclase forms as a result of twin gliding during strain due to a change in the crystal system of these minerals (Shelly, 1993), and is evidence for crystal plastic deformation at high temperature (Juteau & Maury, 2009). The plagioclase inclusions in the clinopyroxene indicate earlier formation of the plagioclase relative to the host mineral (Fig. 9c). The clinopyroxenes constitute 20–25 % of olivine gabbro and are anhedral diopside with Carlsbad twinning. Locally, the clinopyroxene has altered to hornblende. Inclusions of olivine and clinopyroxene also occur in plagioclase (Fig. 9b), indicating earlier formation of the inclusions compared to the plagioclase. Inclusions of clinopyroxene in orthopyroxene indicate formation of the clinopyroxene before orthopyroxene (Fig. 9d).

Petrographic investigations reveal differences in the sequence of crystallization of the minerals in cumulate rocks of ophiolites (Yumul, 1996). Church & Riccio (1977) have suggested the following four sequences of crystallization for the Bay of Island cumulate ophiolite:

(A) olivine + spinel → orthopyroxene → clinopyroxene → plagioclase
(B) olivine + spinel → clinopyroxene → plagioclase → orthopyroxene
(C) olivine + spinel → clinopyroxene → orthopyroxene → plagioclase
(D) olivine + spinel → plagioclase → clinopyroxene → orthopyroxene

The first three trends relate to supra-subduction zones (SSZ), and the fourth to gabbro in mid-ocean ridges. Pearce, Lippard & Roberts (1984) have distinguished SSZ ophiolites from mid-ocean ridge types based on the sequence of crystallization in the cumulate part of the ophiolitic crustal sequence. According to this classification, in the SSZ ophiolites, clinopyroxene, and sometimes orthopyroxene, crystallize earlier than plagioclase, but in the mid-ocean ridge ophiolites, plagioclase crystallizes before clinopyroxene and orthopyroxene. The observed order of crystallization in the cumulate gabbro of the study area can be divided into two groups:

(1) olivine → plagioclase → clinopyroxene → ± orthopyroxene → amphibole
(2) olivine → clinopyroxene → ± orthopyroxene → plagioclase → amphibole

These groups match the crystallization order in the mid-ocean ridge and SSZ ophiolites, respectively

https://doi.org/10.1017/S0016756812000933 Published online by Cambridge University Press

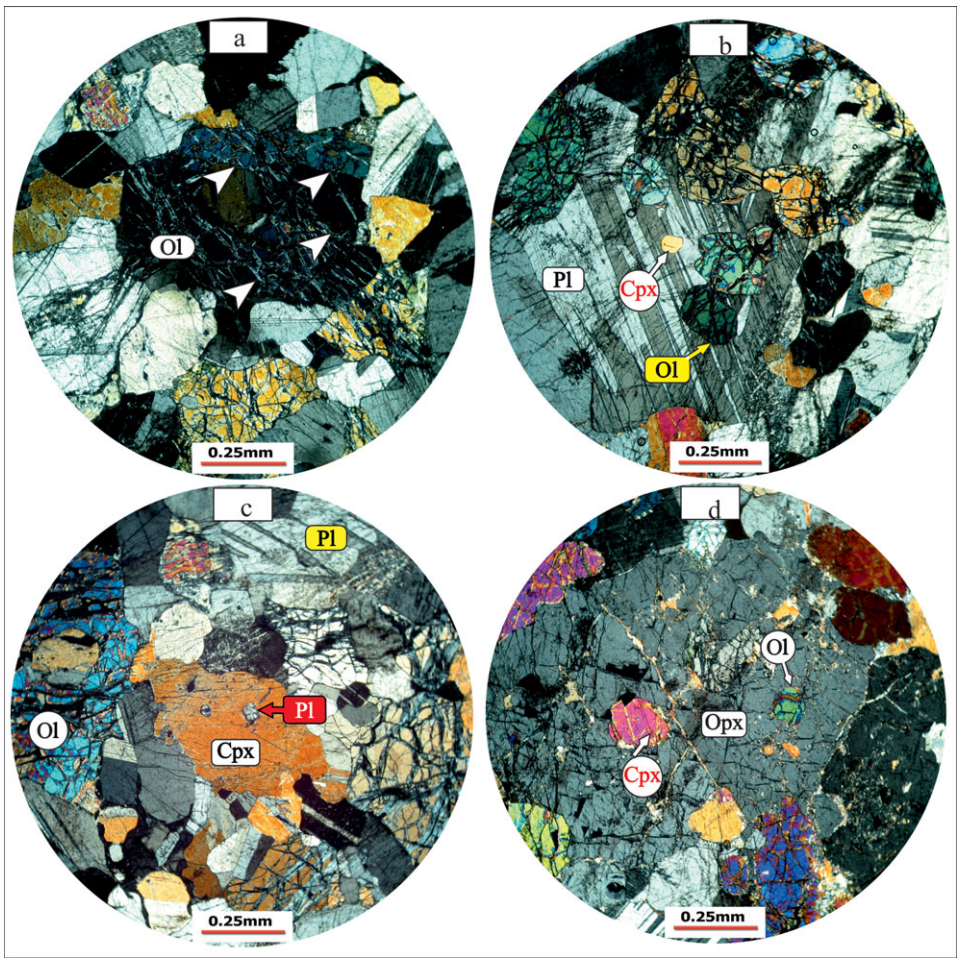

Figure 9. (Colour online) Selected photomicrographs showing: (a) Kink bands in olivine of olivine gabbro, southwest of Soleymanieh. (b) Olivine and clinopyroxene inclusions in plagioclase of olivine gabbro, in which plagioclase shows arrowhead twinning. (c) Plagioclase inclusions in the clinopyroxene of olivine gabbro, southwest of Soleymanieh. (d) Olivine and clinopyroxene inclusions in orthopyroxene. Abbreviations: Ol – olivine, Pl – plagioclase, Cpx – clinopyroxene, Qtz – quartz.

(Cameron, Nesbit & Dietrich, 1980; Hebert & Laurent, 1990; Parlak, Deloye & Bing, 1996; Parlak, Hock & Deloye, 2002; Yamasaki, Maeda & Mizuta, 2006). Orthopyroxene is also an early phase in the cumulate rocks of the SSZ ophiolites, and crystallizes earlier than plagioclase (Cameron, Nesbit & Dietrich, 1980; Pearce, Lippard & Roberts, 1984; Hebert & Laurent, 1990; Parlak, Deloye & Bing, 1996; Parlak, Hock & Deloye, 2000, 2002; Kocak *et al*. 2005; Yamasaki, Maeda & Mizuta, 2006). Perhaps it is for this reason that wehrlite is more common than troctolite in the cumulate part of the SSZ ophiolites (Pearce, Lippard & Roberts, 1984). In general, the order of crystallization is also related to the change in pressure. For example, in subduction zones, where pressure is high, pyroxene crystallizes before plagioclase, whereas in low-pressure environments, such as mid-ocean ridges, plagioclase crystallizes before pyroxene (Parlak, Deloye & Bing, 1996; Parlak, Hock & Deloye, 2002).

The studied pyroxene gabbro displays a mesocumulate texture compared to the pyroxenite, which has an adcumulate texture. Olivine, in the massive gabbro, gradually disappears and, by growing clinopyroxene among the plagioclase, forms mesocumulate (Fig. 10a, b) and heteradcumulate (Fig. 10c) textures. Granular and intergranular textures are seen in the upper parts in the massive and isotropic gabbro, where hornblende also appears as a major mineral. The foliated gabbro reveals adcumulate and heteradcumulate textures (Fig. 10c), with oriented plagioclase and clinopyroxene. Plagioclase is the cumulus phase, and clinopyroxene, orthopyroxene and hornblende constitute the intercumulus mineral phases. The plagioclase has a tabular crystalline form and, in places, zoned albite and albite-Carlsbad twinning. Although these are often intact, they are altered into argillaceous minerals along fractures. Clinopyroxene and orthopyroxene have altered into tremolite-actinolite and hornblende, respectively. Clinopyroxene and orthopyroxene inclusions occur in large hornblende crystals. Intercumulus phase hornblende, clinopyroxene and orthopyroxene surround plagioclase crystals, forming a heteradcumulate texture. Hornblende constitutes about 15 % of the microscopic sections of the foliated, hornblende-bearing gabbro. In the diabase sheeted dyke, small quartz crystals intersperse among other minerals (Fig. 10d). Coarse-grained diabase sheeted dykes display the phyric texture, with a diabase groundmass

https://doi.org/10.1017/S0016756812000933 Published online by Cambridge University Press

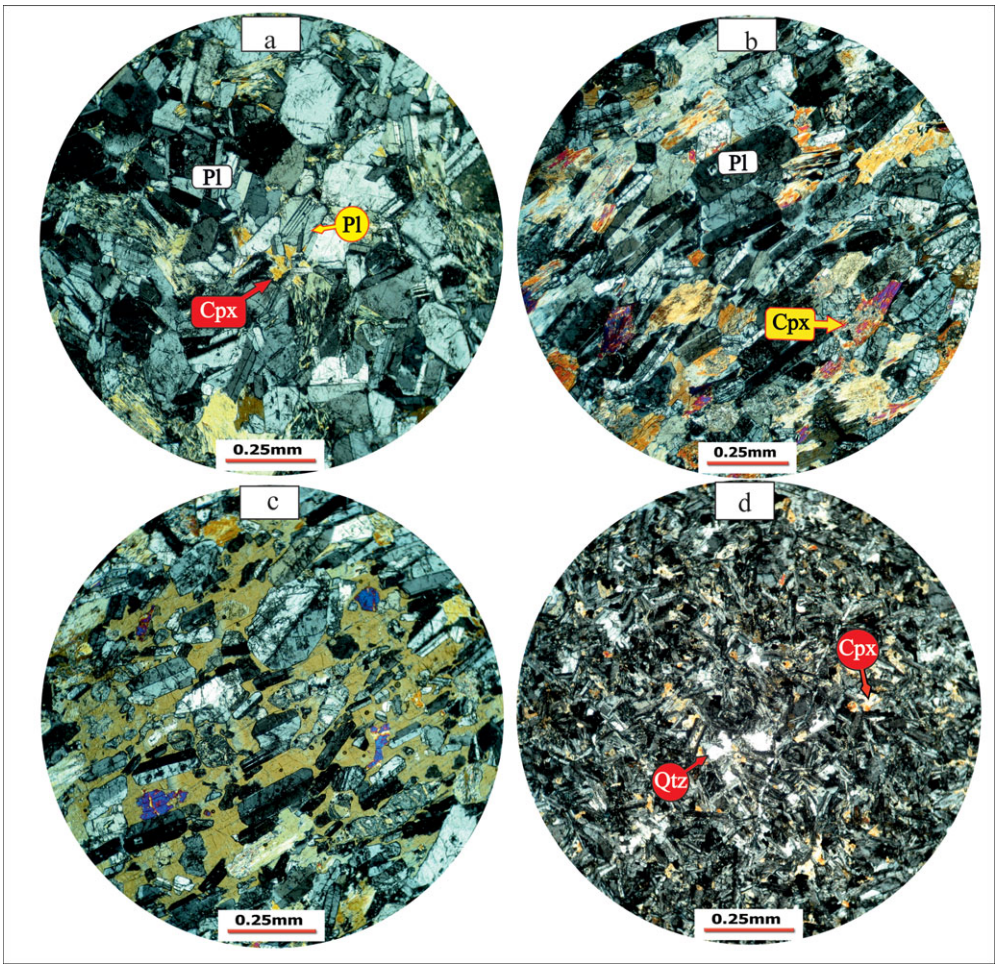

Figure 10. (Colour online) Selected photomicrographs showing: (a, b) Mesocumulate texture in the Garagoli massive gabbro and foliated gabbro, where clinopyroxene occurs between the plagioclase (b). (c) Heteradcumulate texture in the foliated gabbro, north of Garagoli, in which amphibole poikilitically encloses plagioclase. (d) Quartz diabase, north of Garagoli. Abbreviations as in Figure 9.

(Fig. 11a), compared to the fine-grained dykes, which have a diabasic texture (Fig. 11b). Diabasic texture is dominant in the microscopic sections of the diabases. Olivine is minor, and is substituted by serpentine and iddingsite. Clinopyroxene is often substituted with tremolite-actinolite, chlorite and opaque minerals, and plagioclase is substituted by clay minerals. The large crystals in the phyric diabase are often plagioclase and sometimes clinopyroxene.

The presence of the heteradcumulate and mesocumulate textures in the gabbros of the study area indicates an open, pervious magma chamber that led to the formation of oikocrysts that poikilitically enclose the cumulate crystals in the heteradcumulate texture, which is characteristic of the cumulate parts of SSZ (Hunter, 1996; Winter, 2001). The granular texture in these rocks is a result of crystal packing during the compaction process. Hunter (1996) believed that an adcumulate texture can form as a result of a series of diverse processes, including crystal compaction, interconnectedness, enlargement, recrystallization, dissolution and redeposition, which enhance the compaction process. This adcumulate texture is characteristic of an open magmatic system that is common in the SSZ ophiolites (Hunter, 1996; Winter, 2001).

The wehrlite and olivine websterite intrusions have a heteradcumulate texture, showing enclosure of the cumulate olivine by diopside (Fig. 11c). Under the microscope, samples from the wehrlitic intrusion show olivine and clinopyroxene and minor orthopyroxene. Based on the abundance and type of pyroxenes, the wehrlitic intrusion can also be classified as olivine websterite. In some thin-sections, olivine is altered into serpentine, leaving only a small amount of the original mineral in a mesh texture. Clinopyroxene is diopside, which, in less altered samples, covers olivine in a heteradcumulate texture, indicating that the formation of olivine preceded that of clinopyroxene. The absence of plagioclase in the wehrlitic intrusions indicates their formation at high pressures. It seems that these rocks formed as a result of late-stage melting of the refractory parts of the mantle wedge above the subducting slab, and for this reason, they contain abundant olivine (Ernewein, Pflumio & Whitechurch, 1988; Juteau *et al.* 1988; Crawford, Falloon & Green, 1989; Robinson & Malpas, 1990). The plagiogranite has a granular to microgranular texture (Fig. 11d) and the individual dykes have a microgabbroic texture and an andesitic-basaltic composition. The microgabbro has intergranular and ophitic textures, and the andesitic-basaltic dykes have

https://doi.org/10.1017/S0016756812000933 Published online by Cambridge University Press

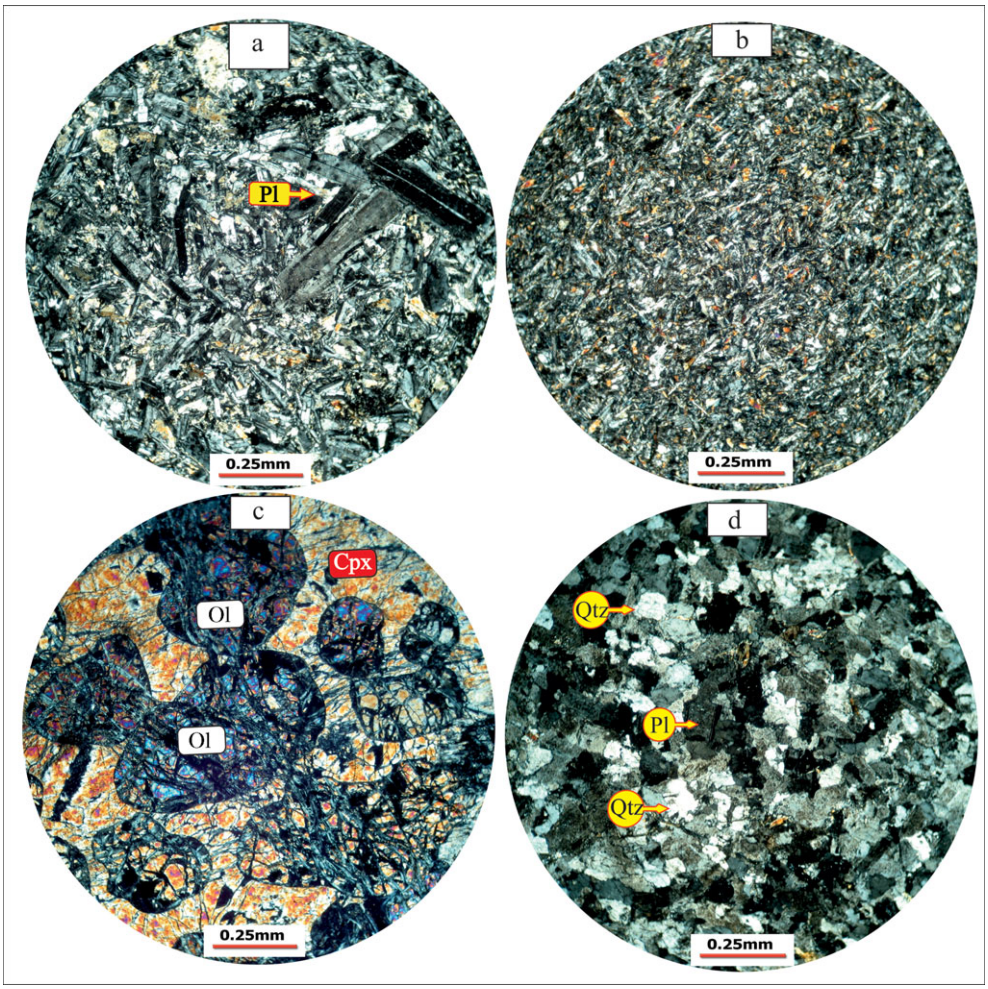

Figure 11. (Colour online) Selected photomicrographs showing: (a) Phyric diabase, north of Garagoli. (b) Microcrystalline diabase, north of Garagoli. (c) Wehrlite with heteradcumulate texture. (d) Microgranular texture in plagiogranite. Abbreviations as in Figure 9.

phyric to glomeroporphyric textures, with a devitrified or hyalomicrolithic groundmass.

4. Geochemistry

The results of the geochemical analyses are given in Table 1. These data are plotted in the classification, spider and tectonomagmatic diagrams, the interpretations of which constitute the basis for the geochemical discussion in this paper. For the geochemical classification, standard diagrams using major oxides or a mixture of major and minor oxides are used. The geochemical data show that the SiO_2 content is 49.6–51.7 % in the cumulate and pyroxene gabbro, 47.5–54.7 % in the massive gabbro, 57.4–59.1 % in the diabase sheeted dykes, and an average of 53.4% in the foliated gabbro (Fig. 12a). In the classification diagram (Middlemost, 1985), based on a variation of Na_2O+K_2O v. SiO_2 (Fig. 12a), samples of the massive gabbro plot in the gabbro field, and those from the foliated hornblende gabbro and individual diabase dykes plot on the border between gabbro and diorite gabbro. Samples from the diabase sheeted dykes plot in the diorite field, and plagiogranite samples plot in the quartz monzonite and granite fields. For a better comparison, the analytical data are plotted on the Winchester & Floyd (1976) diagram, which uses the Nb/Y minor element ratio (Fig. 12b). According to Pearce (1996), the Nb/Y = 0.7 ratio is the value that separates the alkaline and subalkaline series in volcanic rocks. In this diagram, individual diabase dykes plot in the field of subalkaline basalt. Except for one massive gabbro, which plots in the alkali basalt field, the rest of the massive gabbro samples lie in the fields of subalkaline basalt and andesite-basalt. The foliated hornblende gabbro and diabase sheeted dykes plot in the field of andesite-basalt, and the plagiogranite samples plot in the andesite and rhyodacite-dacite fields (Fig. 12b).

The plot of FeO+MgO against SiO_2 (Miyashiro, 1974) (Fig. 12c) shows that all the samples plot in the calc-alkaline field. The ternary $FeO+Fe_2O_3$, Na_2O+K_2O, MgO diagram (Irvine & Baragar, 1971) (Fig. 12d) allows us to discriminate between the tholeiitic and calc-alkaline magmatic series. The analyzed samples show a calc-alkaline and tholeiitic affinity when plotted on this diagram.

Figure 12c, d shows the results of the geochemical analysis applying the magmatic series discrimination diagrams described below. Spider diagrams reveal

https://doi.org/10.1017/S0016756812000933 Published online by Cambridge University Press

Table 1. Geochemical data of the major (%) and minor (ppm) elements in the studied samples

Rock type	weh	weh	weh	cgb	cgb	cgb	pgb	igb	igb	igb
Sample	Sb-53	Sb-56	Sb-59	Sb-48	Sb-41	Sb-42	Sb-14	Sb-18	Sb-23	Sb-24
SiO_2	40.4	44.3	42.5	46.8	49.6	51.7	51.0	54.7	53.5	52.8
TiO_2	0.07	0.19	0.10	0.17	0.12	0.23	0.84	0.29	0.38	0.26
Al_2O_3	4.54	4.52	3.46	7.09	14.9	13.5	19.2	15.2	19.4	24.2
Fe_2O_3t	9.67	7.81	9.30	13.20	5.45	6.86	6.35	7.14	6.04	4.77
MnO	0.15	0.13	0.15	0.20	0.10	0.13	0.09	0.13	0.10	0.08
MgO	> 30	29.2	> 30	23.5	15.8	12.7	7.73	12.3	8.67	6.35
CaO	4.14	7.4	6.1	7.48	7.48	14.3	12.4	13.2	12.3	12.8
Na_2O	< 0.01	0.3	0.2	0.3	0.5	0.7	2.7	1.1	2.2	2.3
K_2O	< 0.01	0.02	0.01	0.01	0.04	0.06	0.08	0.04	0.13	0.09
P_2O_5	< 0.01	< 0.01	< 0.01	< 0.01	< 0.01	< 0.01	0.04	0.02	0.03	0.02
Cr_2O_3	0.17	0.37	0.30	0.18	0.13	0.07	0.05	0.09	0.02	0.01
LOI	8.47	5.52	7.09	1.99	3.10	0.99	3.04	1.25	2.72	3.07
SUM	101.6	99.9	101.6	100.9	104.7	101.2	103.5	> 105	> 105	> 105
V	52	127	88	151	106	175	244	165	148	120
Co	116	94.3	114	117	96.4	35.7	30.1	35.8	26.4	21.5
Ni	1440	1110	1450	995	316	152	151	163	59	48
Cu	12	9	20	25	< 5	58	29	36	18	28
Zn	51	40	46	67	20	27	33	37	20	16
Rb	0.4	0.6	0.3	0.4	0.9	0.4	0.5	0.3	0.7	0.7
Sr	< 10	20	10	60	90	100	260	190	180	230
Y	1.9	5.1	3.3	3.7	2.9	5.2	15.5	7.2	6.6	5.0
Zr	3.4	6.6	5.8	2.5	3.0	5.1	19.7	12.1	14.1	12.5
Nb	< 1	< 1	< 1	< 1	< 1	< 1	< 1	< 1	< 1	< 1
Ba	< 10	10	< 10	< 10	< 10	< 10	10	< 10	10	< 10
Cs	< 0.1	< 0.1	< 0.1	< 0.1	< 0.1	< 0.1	< 0.1	< 0.1	< 0.1	< 0.1
La	0.7	1.0	0.7	0.6	< 0.1	< 0.1	3.4	0.8	< 0.1	1.6
Ce	0.6	1.1	1.0	0.6	0.7	0.7	3.7	2.1	1.9	1.7
Pr	0.06	0.19	0.15	0.09	0.12	0.16	0.71	0.36	0.34	0.31
Nd	0.4	1.2	0.9	0.6	0.8	1.2	3.9	1.9	2.0	1.4
Sm	0.2	0.4	0.2	0.3	0.3	0.4	1.7	0.8	0.7	0.6
Eu	< 0.05	0.16	0.11	0.13	0.09	0.16	0.65	0.31	0.28	0.30
Gd	0.20	0.62	0.45	0.46	0.45	0.86	2.11	1.09	1.01	0.72
Tb	< 0.05	0.10	0.06	0.08	0.06	0.13	0.45	0.20	0.19	0.12
Dy	0.35	0.90	0.53	0.60	0.52	0.94	2.83	1.26	1.21	0.94
Ho	0.05	0.17	0.12	0.14	0.09	0.23	0.60	0.30	0.30	0.20
Er	0.19	0.55	0.36	0.45	0.38	0.62	1.81	0.97	0.88	0.59
Tm	< 0.05	0.07	< 0.05	< 0.05	< 0.05	0.08	0.27	0.11	0.13	0.08
Yb	0.2	0.5	0.3	0.4	0.3	0.5	1.5	0.8	0.8	0.6
Lu	< 0.05	0.06	< 0.05	< 0.05	< 0.05	0.05	0.17	0.11	0.08	0.08
Hf	< 1	< 1	< 1	< 1	< 1	< 1	< 1	< 1	< 1	< 1
Ta	< 0.5	< 0.5	< 0.5	< 0.5	< 0.5	< 0.5	< 0.5	< 0.5	< 0.5	< 0.5
Th	< 0.1	< 0.1	< 0.1	< 0.1	< 0.1	< 0.1	0.1	0.1	0.1	0.1
U	< 0.05	< 0.05	< 0.05	< 0.05	< 0.05	< 0.05	< 0.05	< 0.05	< 0.05	0.05

Rock type	igb	fgb	idd	dia	dia	dia	dia	dia	plg	plg
Sample	Sb-47	Sb-21	Sb-17	Sb-26	Sb-29	Sb-33	Sb-38	Sb-8	Sb-57	Sb-58
SiO_2	47.5	53.4	54.5	57.4	57.9	56.7	57.4	59.1	67.3	64.2
TiO_2	1.22	0.28	0.66	0.67	0.86	0.69	0.81	0.87	0.64	0.88
Al_2O_3	16.2	19.9	16.7	15.7	17.8	18.7	17.4	16.5	14.1	17.8
Fe_2O_3t	8.82	4.34	9.11	7.26	8.56	7.52	7.77	7.26	5.23	0.92
MnO	0.13	0.09	0.16	0.11	0.11	0.13	0.10	0.13	0.04	0.01
MgO	9.56	9.24	10.20	6.91	5.13	5.92	4.68	4.96	1.26	1.04
CaO	8.87	12.70	9.00	8.41	8.00	9.61	7.49	6.53	3.03	3.13
Na_2O	3.5	2.0	1.5	2.8	3.6	2.7	3.8	3.5	5.8	9.7
K_2O	0.23	0.15	0.03	0.11	0.15	0.19	0.19	0.21	0.17	0.02
P_2O5	0.28	0.03	0.03	0.08	0.10	0.07	0.08	0.09	0.15	0.18
Cr_2O_3	0.05	0.03	0.06	0.04	< 0.01	0.02	< 0.01	< 0.01	< 0.01	< 0.01
LOI	5.88	2.45	0.85	2.09	1.43	0.40	1.66	2.72	1.37	0.50
SUM	102.3	104.6	> 102.0	> 100.0	> 101.0	> 102.0	101.4	101.9	99.0	98.3
V	196	149	256	192	206	220	254	252	41	162
Co	34.5	23.4	39.8	26.2	23.3	26.4	22.3	23.9	12.8	4.9
Ni	97	84	170	68	26	62	26	27	8	17
Cu	90	51	118	< 5	22	16	34	48	28	10
Zn	54	26	47	28	15	23	26	39	14	7
Rb	4.9	1.1	< 0.2	0.9	0.7	1.8	0.7	1.2	1.5	0.2
Sr	790	170	200	230	280	190	180	340	180	40
Y	15.2	6.6	8.0	13.1	15.5	13.7	16.5	16.7	37.0	60.8
Zr	92.3	16.3	8.9	36.5	49.0	37.8	52.7	54.2	106	311
Nb	23	< 1	< 1	1	2	1	1	2	2	5
Ba	100	< 10	< 10	20	30	20	20	20	30	< 10
Cs	< 0.1	< 0.1	< 0.1	< 0.1	< 0.1	< 0.1	< 0.1	< 0.1	< 0.1	< 0.1
La	17.8	3.4	2.5	2.9	2.0	19.0	2.8	4.5	5.7	10.0
Ce	35.6	2.7	2.3	5.5	7.6	5.9	6.4	7.6	14.4	27.8

https://doi.org/10.1017/S0016756812000933 Published online by Cambridge University Press

Table 1. Continued

Rock type	igb	fgb	idd	dia	dia	dia	dia	dia	plg	plg
Sample	Sb-47	Sb-21	Sb-17	Sb-26	Sb-29	Sb-33	Sb-38	Sb-8	Sb-57	Sb-58
Pr	4.07	0.40	0.38	0.87	1.17	0.95	1.07	1.19	2.30	4.28
Nd	16.3	1.9	2.1	5.0	5.7	4.5	5.1	6.0	11.8	21.5
Sm	3.4	0.7	0.8	1.4	1.8	1.3	1.9	2.0	3.8	6.4
Eu	1.20	0.31	0.42	0.56	0.69	0.53	0.67	0.70	1.28	1.34
Gd	3.39	0.93	1.25	2.15	2.32	2.00	2.38	2.48	4.98	8.13
Tb	0.50	0.17	0.23	0.33	0.44	0.39	0.47	0.40	0.89	1.48
Dy	3.36	1.14	1.63	2.54	2.74	2.45	2.99	3.05	6.17	10.00
Ho	0.57	0.25	0.33	0.52	0.61	0.54	0.66	0.63	1.36	2.14
Er	1.79	0.80	1.02	1.52	1.82	1.47	1.99	2.06	3.93	6.63
Tm	0.20	0.11	0.15	0.24	0.26	0.22	0.28	0.28	0.56	0.99
Yb	1.5	0.08	1.0	1.5	1.7	1.5	1.8	1.8	3.8	6.5
Lu	0.20	0.08	0.11	0.18	0.23	0.19	0.25	0.22	0.57	0.99
Hf	2	< 1	< 1	1	1	1	2	2	3	8
Ta	1.4	< 0.5	< 0.5	< 0.5	< 0.5	< 0.5	< 0.5	< 0.5	< 0.5	< 0.5
Th	2.6	0.1	< 0.1	0.3	0.4	0.3	0.4	0.4	0.5	1.2
U	0.57	< 0.05	< 0.05	< 0.07	0.14	0.09	0.13	0.14	0.23	0.46

Abbreviations: weh – wehrlite, cgb – cumulate gabbro, pgb – pyroxene gabbro, igb – isotropic gabbro, fgb – foliated gabbro, idd – isolated diabase, dia – diabase sheeted dyke complex, plg – plagiogranite.

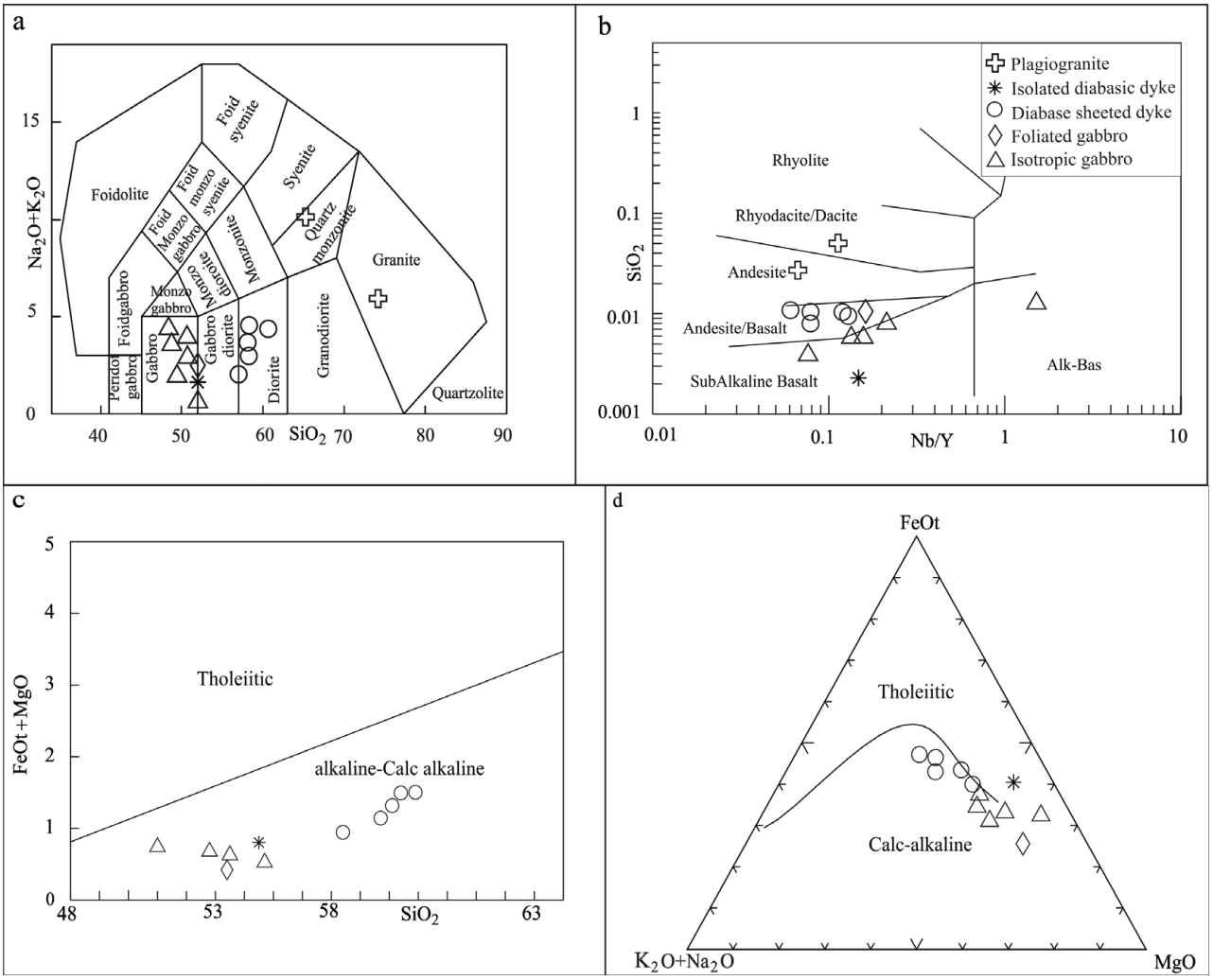

Figure 12. Classification of the studied samples based on the major and minor elements, using (a) Middlemost (1985), (b) Winchester & Floyd (1976), (c) FeOt+MgO against SiO_2 plot (Miyashiro, 1974) and (d) ternary $FeO+Fe_2O_3$, Na_2O+K_2O, MgO diagram (Irvine & Baragar, 1971).

important information about magmatic processes such as differentiation and enrichment or depletion of elements, by normalizing the analytical values to those of standard global values. In this paper, the geochemical data are normalized to the values of primitive mantle and chondrite (Sun & McDonough, 1989) (Figs 13, 14). The REEs in the wehrlite are normalized to the standard chondrite and primitive mantle. The REE pattern in

https://doi.org/10.1017/S0016756812000933 Published online by Cambridge University Press

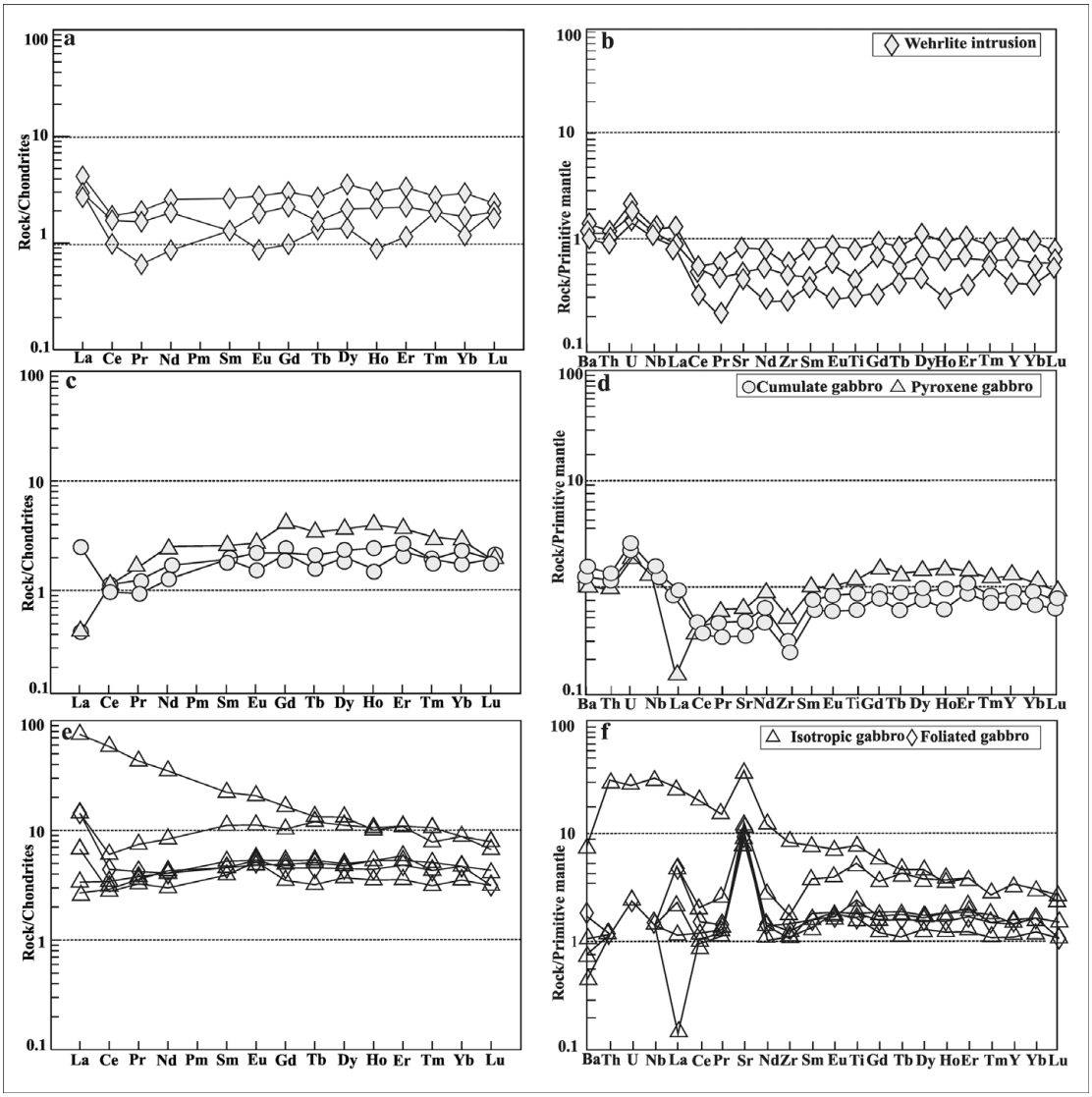

Figures 13. Spider diagrams of the analyzed samples normalized to the standard values of chondrite and primitive mantle (Sun & McDonough, 1989). See text for explanation.

the wehrlite shows depletion in La to Pr, and a 6–30 times linear enrichment from Pr to Lu. These patterns represent low REE values, which may indicate partial melting of a depleted source (Fig. 13a, b).

The patterns of the REEs of the cumulate and pyroxene gabbro, normalized to the standard chondrite (Sun & McDonough, 1989), show a gentle, positive slope of enrichment between La and Sm, and a linear, insignificant slope between Sm and Lu (Fig. 13c). These REE patterns, which vary about four times for the LREEs and five times for the MREEs and HREEs, are similar to the N-MORB patterns at lower levels. Although the cumulate gabbro crystallizes under crystal-mesh conditions, and therefore the concentrations of the REEs are not the same as those in the magma and even in the medium-seated rocks, given the position of the REE patterns of gabbro at low levels, it may be expected that the mantle sources for these rocks were depleted. The REE pattern for pyroxene gabbro lies at a higher level compared to that of the olivine gabbro, probably owing to differentiation.

Patterns of the cumulate and pyroxene gabbro, normalized to the minor and REEs of the standard primitive mantle (Sun & McDonough, 1989), show enrichment in Ba, Th, U and Nd, depletion in La, Ce and Zr, and a linear (horizontal) trend between Sm and Lu (Fig. 13d). Depletion in Ti cannot be seen, indicating that the differentiation and crystallization of the Fe and Ti oxides did not affect the petrogenesis of these rocks (Kocak *et al*. 2005).

The REE patterns of the massive and foliated hornblende gabbro, normalized to the standard values of chondrite (Sun & McDonough, 1989), show enrichment, from 2.5 times to 15 times for the LREEs, and three times to eight times for the HREEs. Except for the Ce depletion, the patterns show a linear variation. Only one massive gabbro sample shows enrichment in the LREEs greater even than the average transitional MORB (T-MORB) field; the rest of the patterns plot in the lower average N-MORB field (Fig. 13e). The enrichment in the LREEs in this pattern, as much as around 100 times, can indicate an enriched mantle

https://doi.org/10.1017/S0016756812000933 Published online by Cambridge University Press

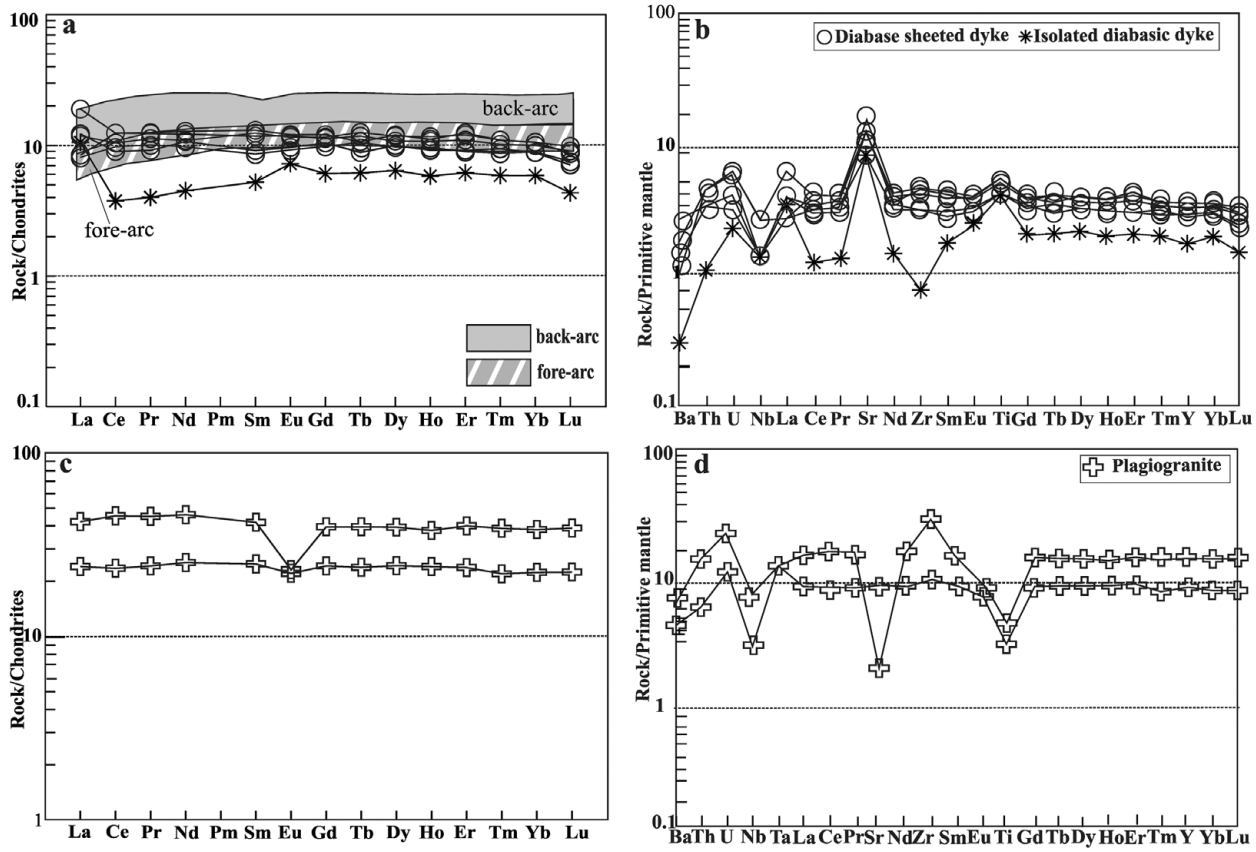

Figure 14. Spider diagrams of the analyzed samples normalized to the standard values of chondrite and primitive mantle (Sun & McDonough, 1989). In (a), the fields for the average fore-arc and back-arc are drawn using data from Nicholson, Black & Picard (2000). See text for explanation.

source. The enrichment in La in some samples may suggest the presence of garnet in the source (Kocak *et al*. 2005). The depletion of Ce relative to La in a few samples may be explained by taking the effect of sea water into account (Hole *et al*. 1984; Saunders & Tarney, 1984). The linear trend of the massive gabbro may be explained by considering the concentration of the MREEs and HREEs in amphiboles (Kocak *et al*. 2005) and the abundance of green hornblende in gabbro.

The spider diagrams of the isotropic gabbro samples, normalized to the chondrite values, reveal three types of pattern. The first shows enrichment relative to the T-MORB values, which may be related to mantle plumes or a garnet-bearing peridotite source. The other two types show ten times and two times enrichments, probably owing to variable degrees of partial melting of peridotite sources or variable enrichment of these sources, which are typical of the SSZ environments (Dilek *et al*. 2003; Martinez & Taylor, 2002; Stern *et al*. 2006; Ishikawa *et al*. 2007; Tian *et al*. 2008; Juteau & Maury, 2009). The REE patterns of the massive and foliated gabbro, normalized relative to the values in the standard primitive mantle (Sun & McDonough, 1989), show enrichment in La in a few samples, and Sr and U in all samples. A depletion in Zr (one sample) and slight depletion in Nb (two samples) can be seen (Fig. 13e). Except for one sample, taken from the massive gabbro, the pattern resembles that of ocean island basalt (OIB), showing a negative slope from the incompatible to the compatible elements. In this pattern, the lower concentrations of the high-field-strength elements (HFSEs) and higher concentration of the large ion lithophile elements (LILEs) relative to those in MORB, can indicate a source of enriched mantle or a mantle plume (Juteau & Maury, 2009).

The fact that only two isotropic gabbro samples reveal a slight Nb depletion in their spider diagram patterns, normalized to the primitive mantle (Sun & McDonough, 1989), and the rest of the samples show linear MORB-like patterns, may be explained by the partial melting of their spinel-bearing peridotite source (Y. Lagabrielle, unpub. Ph.D. thesis, Univ. Bretagne Occidentale, Brest, 1987). Laboratory work by Lin, Stern & Bloomer (1989) has shown that intermittent partial melting of a spinel-bearing peridotite may produce magmas with variable, but linear enrichments. The clear Nb depletion, relative to La and Ce on one side and Th on the other, on chondrite- and primitive mantle-normalized spider diagram patterns of the diabase and plagiogranite samples (Fig. 14), are similar to those identified in the patterns of samples taken from ophiolites in other parts of the world, which have been interpreted to have formed in SSZ environments (Dilek *et al*. 2003; Martinez & Taylor, 2002; Stern *et al*. 2006; Ishikawa *et al*. 2007; Tian *et al*. 2008; Juteau & Mury, 2009).

https://doi.org/10.1017/S0016756812000933 Published online by Cambridge University Press

The geochemical composition of the diabase sheeted dykes provides more effective clues about the geotectonic setting of an ophiolite complex than that of its gabbro and basalt (Nicolas, 1989). The REE patterns of the diabase sheeted dykes, normalized to the standard values of chondrite (Sun & McDonough, 1989), are almost flat, with a minor LREE enrichment compared to the HREEs (Fig. 14a). The fields for the average fore-arc and back-arc are drawn using data from Nicholson, Black & Pickard (2000). These patterns plot at a higher, enriched level than the REE patterns of the cumulate, massive and foliated gabbros, with the LILE concentrations more enriched than the N-MORB, similar to island arc tholeiite (IAT) patterns (Alabaster, Pearce & Malpas, 1982). The abundance of REEs in these samples is about 20 times chondrite for the LREEs and reaches, with a gentle negative slope, about five times chondrite for the HREEs. The higher LREE concentrations, relative to the HREEs, are related to the narrow basins that form above the subduction zone (Saunders & Tarny, 1984). The higher enriched position of the REE patterns of the diabase sheeted dykes, relative to those of the other units of the Bagjer and Garagoli crustal sequence, also supports the idea that these rocks formed through differentiation. The lower concentrations of the HFSEs and higher concentrations of the LILEs relative to MORB probably indicate a depleted mantle source (Taylor & Martinez, 2003; Srivastava, Chandra & Shastry, 2004).

The REE patterns of the individual diabase dykes, normalized to the standard values of chondrite (Sun & McDonough, 1989), are enriched in La (Fig. 14a), and like those of the massive and foliated gabbro plot lower than the patterns of the N-MORB. The Eu enrichment and Ce depletion observed in these patterns are explained above for the case of massive and foliated gabbro. The minor and REE patterns for the diabase sheeted dyke complex and individual diabase dykes, normalized to the standard values of the primitive mantle (Sun & McDonough, 1989), show a small enrichment in the LILEs of Sr, U, La and Th, and depletion in the HFSEs such as Zr (only in individual diabasic dykes) and Nb (Fig. 14b). The patterns for the HFSEs show a general depletion compared to the N-MORB composition. The depletion of Nb and Zr in individual diabasic dykes and enrichment of U indicate partial melting of the source magma from the mantle wedge, which is variably enriched by the fluids originating from the subducting plate and different degrees of partial melting (Hopper & Smith, 1996; Elliot *et al*. 1997; Yunpeng & Bingquan, 2000; Chung *et al*. 2001; Kelemen, Hanghoj & Greene, 2004; Stern *et al*. 2006; Ishikawa *et al*. 2007; Tian *et al*. 2008).

The REE patterns of the plagiogranite samples, normalized to the standard values of chondrite (Sun & McDonough, 1989), are linear, and lie in the average T-MORB field (Fig. 14c). The Eu depletion is observed in only one sample, which can be explained with magmatic differentiation and separation of plagioclase. The minor and REEs for the plagiogranite, normalized to the primitive mantle standard values (Sun & McDonough, 1989), show a clear depletion in Nb and Ti. The scatter in the Rb and Ba values may be explained by the effect of fluids and alteration (Fig. 14d).

As a general conclusion, based on the interpretation of the spider diagrams, it can be said that the depletion in Nb in the patterns of the diabase and plagiogranite, and the slight depletion in Nb in a few patterns of the samples of massive gabbro, are similar to those of the tholeiitic and andesitic basalt of island arcs (Parlak, Hock & Deloye, 2000). The variable enrichment of the LILEs, such as U, and depletion in Nb and Zr could be related to variable degrees of partial melting of the mantle wedge and the effects of different fluids emanating from the underlying subducting slab (Yunpeng & Bingquan, 2000; Chung *et al*. 2001; Taylor & Martinez, 2003; Stern *et al*. 2006; Ishikawa *et al*. 2007; Tian *et al*. 2008). Experimental investigations also suggest enrichment of the above-mentioned elements through fluids that originate from the subducting plate (Ayers, 1998; Chung *et al*. 2001). Moreover, the depletion of some of the HFSEs such as Nb, and their lower values compared to MORB, can be correlated with those of island arc magmas (McChulloch & Gamble, 1991; Pearce & Peate, 1995), indicating that the elements have been preserved through the processes of differentiation and partial melting of the subducting oceanic slab (Pearce, 1996). In subduction environments, the minor refractory phases, such as ilmenite and rutile, are stable in the subducting slab and, as a result, the HFSEs such as Nb, Zr and Ti are preserved, leading to their depletion in the magma that forms as a result of partial melting of the subducting slab (Bogoch, Avigad & Weissbrod, 2002; Nagudi, Koberl & Kurat, 2003).

5. Tectonomagmatic setting

Serri (1981) divided the ophiolitic cumulate gabbro into the high-Ti field (corresponding with mid-ocean ridges) and low-Ti field (corresponding with island arcs) based on the variation of TiO_2 relative to the FeOt/(FeOt+MgO) ratio. Except for two samples taken from the massive gabbro, rocks from the Sabzevar crustal sequence lie in the low-Ti ophiolite field or on its border with the high-Ti ophiolite field on the TiO_2 v. FeOt/(FeOt+MgO) diagram (Fig. 15a).

Figure 15b shows the distribution of the geochemical data on the Na_2O+K_2O, MgO, FeOt ternary diagram (Beard, 1986). Samples from the massive gabbro plot in the arc-related mafic cumulate field, and those of the diabase sheeted dykes plot in the arc-related non-cumulate gabbro and diorite field, all corresponding with the petrographic characteristics observed in these samples. The geochemical distributions of most of these data points correspond with the fields for island arc magmas or the border areas of these fields. Figure 15c shows the distribution of the data points on the V v. Ti/1000 diagram (Shervais, 1982), on which the Miyashita, Adachi & Umino (2003) tectonomagmatic

https://doi.org/10.1017/S0016756812000933 Published online by Cambridge University Press

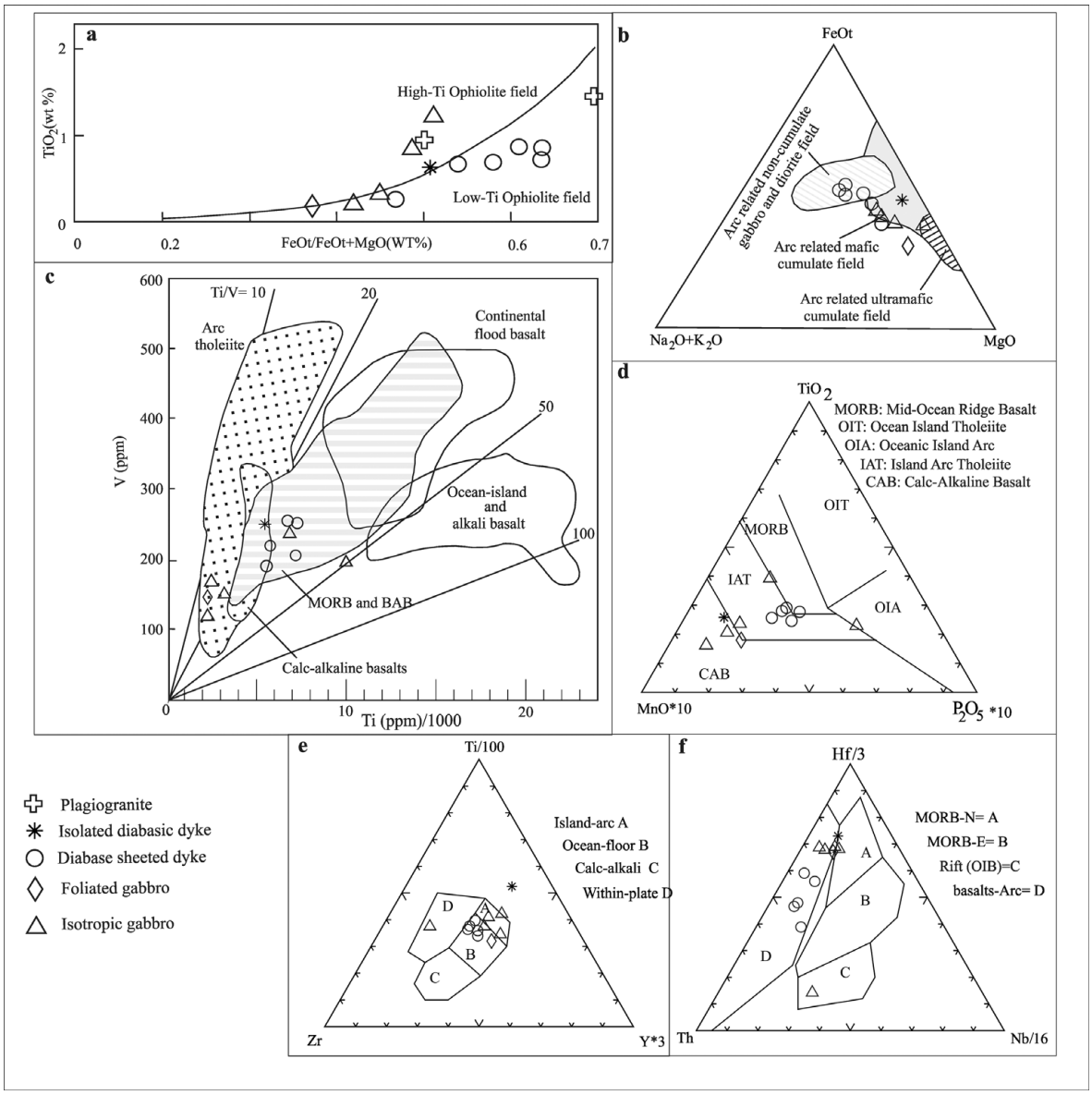

Figure 15. The position of the analyzed samples in various tectonomagmatic diagrams. See text for explanation.

fields are also shown. Samples from the massive gabbro and foliated hornblende gabbro plot in the IAT field on this diagram. The samples from the diabase sheeted and individual dykes, and one sample from the massive gabbro, plot in the MORB field (Fig. 15c). Such a diagram, when used for ophiolites with known origin, reveals that the geochemical data of SSZ ophiolites, such as Zambales in the Philippines, plot in the IAT or MORB fields (Yumul, 1996).

The fields for calc-alkaline basalt (CAB), IAT, ocean island arcs (OIA), MORB and oceanic island tholeiite (OIT) can be distinguished on the $MnO^{*}10$–TiO_2–P_2O_5 major oxides ternary diagram (Mullen, 1983) (Fig. 15d). Samples of the massive gabbro plot in the fields of IAT and CAB on this diagram, and those of the diabase sheeted dykes plot in the IAT field. The fields of the island arc, oceanic floor, calc-alkaline and within-plate basalts are distinguished on the Ti/100–Zr–Y∗3 ternary diagram (Pearce & Cann, 1973). Most of the samples of the massive gabbro plot in the island arc field, and those of the diabase sheeted dykes plot in ocean floor field on this diagram (Fig. 15e). The Th–Hf/3–Nb/16 ternary diagram (Wood, 1980) is used to distinguish the N-MORB, E-MORB, OIB and island arc basalts from each other. Except for one massive gabbro sample, which plots in the OIB field, all samples plot in the island arc basalt field (Fig. 15f).

The investigation of the tectonomagmatic diagrams reveals the compositional diversity of the sampled rocks. The low titanium content of the crustal sequence (Fig. 15a), the position of these rocks in the cumulate and non-cumulate ultramafic and mafic island arc field (Fig. 15b), and the scatter of the data points in the MORB and IAT fields (Fig. 15c, d), suggest that the crustal sequence in the Bagjer–Garagoli and south Soleymanieh areas formed in a subduction zone, or more specifically, a supra-subduction zone (Juteau & Maury, 2009; Parlak, Hock & Deloye, 2000).

https://doi.org/10.1017/S0016756812000933 Published online by Cambridge University Press

6. Discussion and conclusions

The following conclusions may be drawn based on the geological, petrological and tectonomagmatic data presented in this paper. The studied area, located northeast of Sabzevar, is part of the Sabzevar ophiolite belt, which is exposed along the Meyamey Fault that marks the contact between the Central Iran microcontinent and the Alborz–Binalud structural zone. The ophiolite belt includes the mantle and crustal sequences, and a volcanic-sedimentary-volcaniclastic sequence, of which the plutonic crustal sequence is investigated in this paper. The plutonic, crustal sequence includes cumulate, massive and istotropic gabbro and a diabase sheeted dyke complex, which are cut by wehrlite and plagiogranite intrusions and individual micrograbbroic, diabasic and andesitic dykes. The plutonic, crustal sequence constitutes tectonic slices that have thrust over serpentinized peridotite south of Garagoli village, and are thrust over by peridotite north of Bagjer village.

Assuming that the banding in the layered gabbro forms perpendicular to the mid-ocean ridge, and that the diabase sheeted dykes, wehrlite intrusions and plagiogranite dykes form parallel to the ridge, the orientation data of these features suggest an E–W opening north of Garagoli village, and a N–S opening south of the Soleymanieh village. However, it is also possible that the orientations in the Soleymanieh area were rotated by transform or younger faults during emplacement of the ophiolite. Drawing a definite conclusion about the direction of the opening across the mid-ocean ridge in the Sabzevar ophiolite requires taking extensive structural measurement of foliation and lineation in the area between the town of Fariman, in the eastern part of the belt, and the village of Abbasabad in the west.

Palaeontological study of the pelagic limestone, intercalated with pillow lavas, hyaloclastite and hyaloclastic breccia with carbonate cement, gives a Late Cretaceous (Maastrichtian – Late Maastrichtian) age for these rocks and the ophiolite. The presence of isotropic and layered gabbro with cumulate characteristics, the widespread nature of the diabase sheeted dyke complex, the occurrence of wehrlite intrusions and veinlets and dykes of plagiogranite, and the harzburgitic to clinopyroxene harzburgitic composition of the plutonic, crustal sequence, all suggest that the sequence, and probably the Sabzevar ophiolite belt as a whole, formed with a fast spreading rate during the Late Cretaceous. The 'olivine → plagioclase → clinopyroxene → ± orthopyroxene → amphibole', and 'olivine → clinopyroxene → ± orthopyroxene → plagioclase → amphibole' orders of mineralization in the cumulate olivine gabbro represent crystallization in a mid-ocean ridge and SSZ, respectively. The heteradcumulate and mesocumulate textures in the gabbros suggest the presence of an open and porous magma chamber, typical of the SSZ environment. The heteradcumulate texture, which is dominant in the wehrlite intrusions in which plagioclase did not form, suggests crystallization in subduction zones. It seems that these rocks formed as a result of late-stage melting of the refractory parts of the mantle wedge above the subducting slab; which is perhaps the reason why olivine is so abundant in them.

The discrimination diagrams indicate calc-alkaline and tholeiitic affinities for the studied samples. The majority of the samples represent low TiO_2 gabbro, suggesting either a heterogeneous harzburgitic source or crystallization under high pressure. The high MgO values in the cumulate gabbro and wehrlite suggest either a high percentage of partial melting in the mantle source or a high magnesium source. The fact that the cumulate gabbro and diabase have the highest and lowest Cr_2O_3 content, respectively, can be explained by the decrease in the crystallization of clinopyroxene in the diabase. The low amounts of HFSEs, such as Zr, Y and Nb, in some samples with cumulate characteristics, suggest a higher participation of the cumulus minerals compared to the intercumulus liquid. The spider diagram patterns of a significant number of studied samples resemble those of the IAT and andesitic basalts. Variable enrichment, even in insignificant amounts, of the LILEs, e.g. U, and depletion in Nb and Zr, can be attributed to variable degrees of partial melting of the mantle wedge and the effects of the fluids emanating from the underlying, subducting slab. The depletion of some of the HFSEs, such as Nb, in some of the patterns, and their positions at lower levels, in the average MORB field, can be compared with that of volcanic arc magmas. The tectonomagmatic diagrams indicate that most of the samples taken from the plutonic crustal sequence represent the low-Ti series or the border line between the fields of low- and high-Ti series. The positioning of the samples in different fields of the tectonomagmatic diagrams reflects the variability in rock composition. In addition to the low Ti content of most of the studied samples, their positioning in the cumulate ultramafic and mafic fields and non-cumulate arc field, and their distribution between MORB and tholeiitic arc, indicate formation of the plutonic, crustal sequence in relation to subduction and, more specifically, to supra-subduction.

Acknowledgements. We thank Dr Ghasemi and Mr Safar Ali Eshraghi for field logistics, and Ms Zohre Sohrabi for the palaeontological investigation of the thin-sections. We thank Drs Thierry Juteau and Scott Whattam for their thorough and constructive reviews of the original manuscript, which led to significant improvement of the paper.

References

ANONYMOUS. 1972. Penrose field conference on ophiolites. *Geotimes* **17**, 24–5.

AGHANABATI, A. 2004. *Major Sedimentary-Structural Units of Iran*. Geological Survey of Iran.

ALABASTER, T., PEARCE, J. A. & MALPAS, J. 1982. The volcanic stratigraphy and petrogenesis of the Oman ophiolite complex. *Contributions to Mineralogy and Petrology* **81**, 168–83.

AYERS, J. 1998. Trace element modeling of aqueous fluid peridotite interaction in the mantle wedge of subduction zone. *Contributions to Mineralogy and Petrology* **132**, 390–404.

BAROZ, F., MACAUDIÈRE, J., MONTIGNY, R., NOGHREYAN, M., OHNENSTETTER, M. & ROCCI, G. 1984. Ophiolites and related formations in the central part of the Sabzevar Range (Iran), and possible geotectonic reconstruction. *Neues Jahrbuch für Geologie und Paläontologie – Abhandlungen* **168**, 358–88.

BEARD, J. S. 1986. Characteristic mineralogy of arc-related cumulate gabbros: implications for the tectonic setting of gabbroic plutons and for andesite genesis. *Geology* **14**, 848–51.

BOGOCH, R., AVIGAD, D. & WEISSBROD, T. 2002. Geochemistry of the quartz diorite granite association, Roded area, southern Israel. *Journal of African Earth Sciences* **35**, 51–9.

CAMERON, W. E., NESBIT, E. G. & DIETRICH, V. J. 1980. Petrographic dissimilarities between ophiolite and ocean floor basalts. In *Ophiolites: Proceedings of the International Ophiolite Symposium, Cyprus 1979* (ed. A. Panayiotou), pp. 182–92. Nicosia: Cyprus Geological Survey Department.

CHUNG, S.-L., WANG, K.-L., CRAWFORD, A. J., KAMENETSTY, V. S., CHEN, C.-H., LAN, C.-Y. & CHEN, C.-H. 2001. High Mg potassic rocks from Taiwan: implications for the genesis of orogenic potassic lavas. *Lithos* **59**, 153–70.

CHURCH, W. R. & RICCIO, L. 1977. Fractionation trends in the Bay of Islands ophiolite of Newfoundland: polycyclic cumulate sequences in ophiolites and their classification. *Canadian Journal of Earth Science* **14**, 1156–65.

CRAWFORD, A. J., FALLOON, T. J. & GREEN, D. H. 1989. Classification, petrogenesis, and tectonic setting of boninites. In *Boninites and Related Rocks* (ed. A. J. Crawford), pp. 2–49. Boston, Mass.: Unwin Hyman.

DILEK, Y. 2003. Ophiolite pulses, mantle plumes and orogeny. In *Ophiolites in Earth History* (eds Y. Dilek & R. T. Robinson), pp. 9–19. Geological Society of London, Special Publication no. 218.

ELLIOTT, T., PLANK, T., ZINDLER, A., WHITE, W. & BOURDON, B. 1997. Element transport from slab to volcanic front at the Mariana arc. *Journal of Geophysical Research* **102**, 14991–5019.

EMAMI, M. H., SADEGI, M. M. & OMRANI, S. J. 1993. *Magmatic Map of Iran, Scale 1:1,000,000*. Geological Survey and Mining Exploration of Iran.

ERNEWEIN, M., PFLUMIO, C. & WHITECHURCH, H. 1988. The death of an accretion zone as evidenced by the magmatic history of the Sumail Ophiolite (Oman). In *The Ophiolites of Oman* (eds F. Boudier & A. Nicolas). *Tectonophysics* **151**, 247–74.

HEBERT, R. & LAURENT, R. 1990. Mineral chemistry of the plutonic section of the Troodos Ophiolite: new constraints for genesis of arc-related ophiolites. In *Ophiolites: Oceanic Crustal Analogues, Proceedings of the "Troodos 1987" Symposium* (eds J. Malpas, E. M. Moores, A. Panayiotou & C. Xenophontos), pp. 149–63. Nicosia, Cyprus: Geological Survey of Cyprus.

HOLE, M. J., SAUNDERS, A. D., MARRINER, G. F. & TARNEY, J. 1984. Subduction of pelagic sediments: implications for the origin of Ce anomalous basalts from the Mariana Islands. *Journal of Geological Society, London* **141**, 453–72.

HOPPER, D. J. & SMITH, I. M. 1996. Petrology of the gabbro and sheeted basaltic intrusives at North Cape, New Zealand. *New Zealand Journal of Geology and Geophysics* **39**, 389–402.

HUNTER, R. H. 1996. Texture development in cumulate rocks. In *Layered Intrusions* (ed. R. G. Cawthorn), pp. 77–101. Amsterdam: Elsevier.

IRVINE, T. N. & BARAGAR, W. R. A. 1971. A guide to the chemical classification of the common volcanic rocks. *Canadian Journal of Earth Science* **8**, 523–48.

ISHIKAWA, A., KANEKO, Y., KADARUSMAN, A. & OTA, T. 2007. Multiple generations of forearc mafic–ultramafic rocks in the Timor–Tanimbar ophiolite, eastern Indonesia. *Gondwana Research* **11**, 200–17.

JUTEAU, T., ERNEWIN, M., REUBER, I., WHITECHURCH, H. & DAHL, R. 1988. Duality of magmatism in the plutonic sequence of the Sumail nappe, Oman. *Tectonophysics* **151**, 107–35.

JUTEAU, T. & MAURY, R. 2009. *La Croute Océanique: Pétrologie et Dynamique Endogene*. Paris: Société Géologique de France/Vuibert, 470 pp.

KELEMEN, P. B., HANGHOJ, K. & GREENE, A. R. 2004. One view of the geochemistry of subduction related magmatic arcs, with an emphasis on primitive andesite and lower crust. *Treatise on Geochemistry* **3**, 593–659.

KNIPPER, A. & RICOU, L. E. 1986. Ophiolites as indicators of the geodynamic evolution of the Tethyan Ocean. *Tectonophysics* **123**, 213–40.

KOCAK, K., ISIKA, F., ARSLANB, M. & ZEDEF, V. 2005. Petrological and source region characteristics of ophiolitic hornblende gabbros from the Aksaray and Kayseri regions, central Anatolian crystalline complex, Turkey. *Journal of Asian Earth Sciences* **25**, 883–91.

LENSCH, G. 1980. Major element geochemistry of the ophiolites in north-eastern Iran. In *Ophiolites: Proceedings of the International Ophiolite Symposium, Cyprus 1979* (ed. A. Panayotou), pp. 398–401. Nicosia: Cyprus Geological Survey Department.

LENSCH, G. & DAVOUDZADEH, M. 1982. Ophiolites in Iran. *Neues Jahrbuch für Geologie und Paläontologie – Monatshefte* **5**, 306–20.

LENSCH, G., MIHM, A. & ALAVI-TEHRANI, N. 1977. Petrography and geology of the ophiolite belt north of Sabzevar/Khorasan (Iran). *Neues Jahrbuch für Mineralogie – Abhandlungen* **131**, 156–78.

LENSCH, G., MIHM, A. & ALAVI-TEHRANI, N. 1979. Major element geochemistry of the ophiolites north of Sabzevar (Iran). *Neues Jahrbuch für Geologie und Paläontologie – Monatshefte* 415–47.

LENSCH, G., MIHM, A. & ALAVI-TEHRANI, N. 1980. The postophiolitic volcanism north of Sabzevar/Iran: geology, petrography and major element geochemistry. *Neues Jahrbuch für Geologie und Paläontologie – Monatshefte* 686–702.

LIN, P. N., STERN, R. J. & BLOOMER, S. H. 1989. Shoshonitic volcanism in the northern Mariana arc: 2. Large-ion lithophile and rare element abundances: evidence for the source of incompatible element enrichments in intraoceanic arcs. *Journal of Geophysical Research* **94**, 4497–514.

LINDENBERG, H. G., GORLER, K. & IBBEKEN, H. 1983. *Stratigraphy, structure and orogenic evolution of the Sabzevar zone in the area of Oryan (Khorasan, NE Iran)*. Geological Survey of Iran, Geodynamic Project (Geotraverse) in Iran, Report no. 51, pp. 119–143.

MAJIDI, J. 1999. *Sabzevar Geological Map and Report, 1:100,000*. Geological Survey and Mining Exploration of Iran.

MARTINEZ, F. & TAYLOR, B. 2002. Mantle wedge control on back-arc crustal accretion. *Nature* **416**, 417–20.

McCulloch, M. T. & Gamble, J. A. 1991. Geochemical and geodynamical constraints on subduction magmatism. *Earth and Planetary Science Letters* **102**, 358–74.

Middlemost, E. A. K. 1985. *Magmas and Magmatic Rocks: An Introduction to Igneous Petrology*. London: Longman, 266 pp.

Miyashiro, A. 1974. Volcanic rock series in island arcs and active continental margins. *American Journal of Science* **274**, 321–55.

Miyashita, S., Adachi, Y., Umino, S. 2003. Along-axis magmatic system in the northern Oman ophiolite: implications of compositional variation of the sheeted dike complex. *Geochemistry, Geophysics, Geosystems* **4**, 8617, doi:10.1029/2001GC000235, 26 pp.

Mullen, E. D. 1983. $MnO/TiO_2/P_2O_5$: a minor element discriminant for basaltic rocks of oceanic environments and its implications for petrogenesis. *Earth and Planetary Science Letters* **62**, 53–62.

Nagudi, N. O., Koberl, C. H. & Kurat, G. 2003. Petrography and geochemistry of the Singo granite, Uganda and implications for its origin. *Journal of African Earth Sciences* **35**, 51–9.

Nicholson, K. N., Black, P. M. & Picard, C. 2000. Geochemistry and tectonic significance of the Tangihua ophiolite complex, New Zealand. *Tectonophysics* **321**, 1–15.

Nicolas, A. 1989. *Structures of Ophiolites and Dynamics of Oceanic Lithosphere. Petrology and Structural Geology*. Dordrecht, Boston, London: Kluwer Academic Press, 367 pp.

Nicolas, A. & Boudier, F. 2009. Subsidence in magma chamber and the development of magmatic foliation in Oman ophiolite gabbros. *Earth and Planetary Science Letters* **284**, 76–87.

Ohnenstetter, M. 1983. The role of possible transverse faults in the development of the Sabzevar ophiolites, northeast Iran, with special reference to magma chamber tectonics. *Sciences Géologiques Bulletin* **36**, 73–90.

Parlak, O., Delaloye, M. & Bing, L E. 1996. Mineral chemistry of ultramafic and mafic cumulates as an indicator of the arc-related origin of the Mersin ophiolite (southern Turkey). *Geologische Rundschau* **85**, 647–61.

Parlak, O., Hock, V. & Delaloye, M. 2000. Supra-subduction zone origin of the Pozantl-Karsanti Ophiolite (southern Turkey) deduced from whole-rock and mineral chemistry of the gabbroic cumulates. In *Tectonics and Magmatism in Turkey and the Surrounding Area* (eds E. Bozkurt, J. A. Winchester & J. D. A. Piper), pp. 219–34. Geological Society of London, Special Publication no. 173.

Parlak, O., Hock, V. & Delaloye, M. 2002. The supra-subduction zone Pozanti–Karsanti ophiolite, southern Turkey: evidence for high-pressure crystal fractionation of ultramafic cumulates. *Lithos* **65**, 205–24.

Pearce, J. A. 1996. A user's guide to basalt discrimination diagrams. In *Trace Element Geochemistry of Volcanic Rocks: Applications for Massive Sulphide Exploration* (ed. D. A. Wyman), pp. 79–113. Geological Association of Canada, Short Course Notes no. 12.

Pearce, J. A. & Cann, J. R. 1973. Tectonic setting of basic volcanic rocks determined using trace element analyses. *Earth and Planetary Science Letters* **19**, 290–300.

Pearce, J. A., Lippard, S. J. & Roberts, S. 1984. Characteristics and tectonic significance of suprasubdution zone ophiolite. In *Marginal Basin Geology* (eds B. P. Kokelaar & M. F. Howells), pp. 77–94. Geological Society of London, Special Publication no. 16.

Pearce, J. A. & Peate, D. W. 1995. Tectonic implications of the composition of volcanic arc magmas. *Annual Review of Earth and Planetary Sciences* **23**, 251–85.

Robinson, P. T. & Malpas, J. 1990. The Troodos ophiolite: new perspective on its origin and emplacement. In *Ophiolites: Oceanic Crustal Analogues. Ophiolites: Oceanic Crustal Analogues, Proceedings of the "Troodos 1987" Symposium* (eds J. Malpas, E. M. Moores, A. Panayiotou & C. Xenophontos), pp. 13–26. Nicosia, Cyprus: Geological Survey of Cyprus.

Rossetti, F., Nasrabady, M., Vignaroli, G., Theye, T., Gerdes, A., Razavi, M. H. & Moin Vaziri, H. 2009. Early Cretaceous migmatitic mafic granulites from the Sabzevar range (NE Iran): implications for the closure of the Mesozoic peri-Tethyan oceans in central Iran. *Terra Nova* **22**, 26–34.

Sahandi, M. 1992. *Geological Map of Sabzevar*. Geological Survey and Mining Exploration of Iran.

Saunders, A. D. & Tarney, J. 1984. Geochemical characteristics of basaltic volcanism within backarc basins. In *Marginal Basin Geology* (B. P. Kokelaar & M. F. Howells), pp. 59–76. Geological Society of London, Special Publication no. 16.

Serri, G. 1981. The petrochemistry of ophiolitic gabbroic complexes: a key for the classification of gabbroic cumulates into low-Ti and high-Ti type. *Earth and Planetary Science Letters* **52**, 203–12.

Shelley, D. 1993. *Igneous and Metamorphic Rocks Under the Microscope. Classification, Textures, Microstructures, and Mineral Preferred Orientation*. London: Chapman and Hall, 445 pp.

Shervais, J. W. 1982. Ti-V plots and the petrogenesis of modern and ophiolitic lavas. *Earth and Planetary Science Letters* **59**, 101–18.

Spices, G., Lensch, G. & Miham, A. 1983. *Geochemistry of the post-ophiolitic Tertiary volcanic between Sabzevar and Quchan (NE Iran)*. Geological Survey of Iran, Geodynamic Project (Geotraverse) in Iran, Report no. 51, pp. 247–67.

Srivastava, R. K., Chandra, R. & Shastry, A. 2004. High-Ti type N-MORB parentage of basalts from the south Andaman ophiolite suite, India. *Proceedings of the Indian Academy of Science (Earth and Planetary Science)* **113**, 605–18.

Shojaat, B., Hassanipak, A. A., Mobasher, K. & Ghazi, A.M. 2002. Petrology, geochemistry and tectonics of the Sabzevar ophiolite, North Central Iran. *Journal of Asian Earth Sciences* **21**, 1053–67.

Stern, R. J., Kohut, E. J., Bloomer, S. H., Leybourne, M., Fouch, M. & Vervoot, J. 2006. Subduction factory processes beneath the Guguan cross-chin, Mariana Arc: no role for sediments, are serpentinites important? *Contributions to Mineralogy and Petrology* **151**, 202–21.

Stocklin, J. 1968. Structural history and tectonics of Iran: a review. *American Association of Petroleum Geologists Bulletin* **52**, 1229–58.

Sun, S. S. & McDonough, W. F. 1989. Chemical and isotopic systematics of ocean basalts: implications for mantle composition and processes. In *Magmatism in the Ocean Basins* (eds A. D. Saunders & M. J. Norry), pp. 313–46. Geological Society of London, Special Publication no. 42.

Taylor, B. & Martinez, F. 2003. Back-arc basin basalt systematics. *Earth and Planetary Science Letters* **210**, 481–97.

Tian, L., Castillo, P. R., Hawkins, J. W., Hilton, D. R., Hanan, B. B. & Piatruszka, A. J. 2008. Major and

trace element and Sr–Nd isotope signatures of lavas from the Central Lau Basin: implications for the nature and influence of subduction components in the back-arc mantle. *Journal of Volcanology and Geothermal Research* **178**, 657–70.

WAGER, L. R. 1963. The mechanism of adcumulus growth in the layered series of the Skaergaard intrusion. *Special Publication of the Mineralogical Society of America* **1**, 1–19.

WAGER, L. R. & BROWN, G. M. 1968. *Layered Igneous Rocks*. Edinburgh: Oliver and Boyd, 588 pp.

WAGER, L. R., BROWN, G. M. & WADSWORTH, W. J. 1960. Types of igneous cumulate. *Journal of Petrology* **1**, 73–85.

WINTER, J. D. 2001. *An Introduction to Igneous and Metamorphic Petrology*. Upper Saddle River, New Jersey: Prentice Hall Inc., 697 pp.

WINCHESTER, J. A. & FLOYD, P. A. 1976. Geochemical magma type discrimination: application to altered and metamorphosed basic igneous rocks. *Earth and Planetary Scientific Letters* **28**, 459–69.

WOOD, D. A. 1980. The application of a Th-Hf-Ta diagram to problems of tectonomagmatic classification and to establishing the nature of crustal contamination of basaltic lavas of the British Tertiary volcanic province. *Earth and Planetary Scientific Letters* **50**, 11–30.

YAMASAKI, T., MAEDA, J. & MIZUTA, T. 2006. Geochemical evidence in clinopyroxenes from gabbroic sequence for two distinct magmatisms in the Oman ophiolite. *Earth and Planetary Science Letters* **251**, 52–65.

YUMUL, G. P. Jr. 1996. Review of the geochemistry of mid ocean ridge and supra-subduction zone ophiolites: comparison and discussion. *Journal of the Geological Society of the Philippines* **51** (1–2), 3–36.

YUNPENG, D. & BINGQUAN, Z. 2000. Characteristics of the island-arc pillow lavas from southeast Yunnan Province, and its tectonic implications for Paleo-Tethys in South China. *Chinese Science Bulletin* **45** (8), 18–27.